Title: Distinct mechanisms of non-autonomous UPR^{ER} mediated by GABAergic, glutamatergic, and octopaminergic neurons.

Aeowynn J. Coakley[1,*], Adam Hruby[1,*], Jing Wang[1], Andrew Bong[1], Tripti Nair[1], Carmen M. Ramos[1], Athena Alcala[1], Maxim Averbukh[1], Naibedya Dutta[1], Darius Moaddeli[1], Daniel Hicks[1], Mattias de los Rios Rogers[2], Arushi Sahay[3], Sean P. Curran[1], Peter J. Mullen[4], Bérénice A Benayoun, Gilberto Garcia[1,^], Ryo Higuchi-Sanabria[1,^].

[1]Leonard Davis School of Gerontology, University of Southern California, Los Angeles, CA 90089, United States.
[2]Department of Molecular, Cell, and Developmental Biology, University of California, Los Angeles, CA 90095, United States.
[3]Department of Cell & Molecular Biology, University of Pennsylvania, Philadelphia, PA 19104, United States.
[4]Department of Molecular Microbiology and Immunology, Keck School of Medicine, University of Southern California, Los Angeles, CA 90089, United States.
*These authors contributed equally to the work.
^Correspondence to ryo.sanabria@usc.edu, ggarcia1@usc.edu

Keywords: Aging, stress, ER, neurons.

Abstract

The capacity to deal with stress declines during the aging process, and preservation of cellular stress responses is critical to healthy aging. The unfolded protein response of the endoplasmic reticulum (UPR^{ER}) is one such conserved mechanism, which is critical for the maintenance of several major functions of the ER during stress, including protein folding and lipid metabolism. Hyperactivation of the UPR^{ER} by overexpression of the major transcription factor, *xbp-1s*, solely in neurons drives lifespan extension as neurons send a neurotransmitter-based signal to other tissue to activate UPR^{ER} in a non-autonomous fashion. Previous work identified serotonergic and dopaminergic neurons in this signaling paradigm. To further expand our understanding of the neural circuitry that underlies the non-autonomous signaling of ER stress, we activated UPR^{ER} solely in glutamatergic, octopaminergic, and GABAergic neurons in *C. elegans* and paired whole-body transcriptomic analysis with functional assays. We found that UPR^{ER}-induced signals from glutamatergic neurons increased expression of canonical protein homeostasis pathways and octopaminergic neurons promoted pathogen response pathways, while minor, but statistically significant changes were observed in lipid metabolism-related genes with GABAergic UPR^{ER} activation. These findings provide further evidence for the distinct role neuronal subtypes play in driving the diverse response to ER stress.

Introduction

Regulation of organelle homeostasis is essential for maintenance of cellular health, which has direct implications in organismal health and longevity. The endoplasmic reticulum (ER) is one such organelle, which processes about a third of the proteins and lipids in cells and has dedicated quality control machineries to preserve these and numerous other functions. One primary quality control machinery is the ER unfolded protein response (UPR^{ER}), a transcriptional response to ER damage or stress, which activates genes essential for maintenance of proper ER function [1]. Activation of the UPR^{ER} involves the ER-membrane protein, inositol-requiring enzyme 1 (IRE-1), which dimerizes upon sensing ER stress to splice X-box binding protein

(*xbp-1*) mRNA into *xbp-1s*. *xbp-1s* mRNA encodes a functional transcription factor, XBP-1s, which activates genes essential for restoring ER homeostasis, including protein chaperones, autophagy, ubiquitin proteosome system, among others. This transcriptional response to stress is essential for maintaining proper function of the ER and has direct implications in longevity. Specifically, UPR^{ER} function has been shown to decline with age, and heightened activation of UPR^{ER} maintained stress resilience at old age in *C. elegans* [2].

Overexpression of *xbp-1s* solely in neurons is sufficient to enhance *C. elegans* lifespan due to the whole-body activation UPR^{ER} through neuron-to-body communication medicated by neurotransmitter signaling [2]. Upon neuronal UPR^{ER} activation, a complex signaling event mediated by a combination of dopamine, serotonin [3], and tyramine [4], results in dramatic remodeling of peripheral cells. Specifically, intestinal cells can activate proteostasis [4], lipid metabolism [5,6], and lysosomal function [7] to drive longevity. These studies revealed numerous neuronal subtypes and distinct mechanistic pathways, including chaperone induction downstream of serotonergic signaling, lipid remodeling through lipophagy downstream of dopaminergic signaling, and proteostasis machinery through tyramine signaling from RIM and RIC neurons, all of which are essential to promote longevity. Finally, this UPR^{ER} signaling is not limited to neurons, as a recent study revealed several glial subtypes were also capable of eliciting a glia-to-body UPR^{ER} signaling event to promote longevity [8].

Similar homeostatic benefits of UPR^{ER} in neurons are observed in mammals, wherein *Xbp1s* expression in pro-opiomelanocortin (POMC) neurons has been shown to protect against diet-induced obesity by improving leptin and insulin sensitivity under ER stress [9]. While all these studies utilized an artificial transgenic expression system, two recent studies have shown that neuron-to-body UPR^{ER} signaling is an essential signaling pathway for endogenous pathways. In mice, olfactory perception of food is sufficient to promote POMC *Xbp1s* expression and activation of post-prandial liver ER adaption [10]. In *C. elegans*, chemosensation of pathogenic bacteria was found to promote neuronal *xbp1-s* expression, leading to UPR^{ER} activation in peripheral tissues and extension of lifespan [11]. These studies revealed that endogenous neuron-to-body signaling utilized similar mechanistic pathways to *xbp-1s* overexpression paradigms, which highlight the translatability of using transgenic approaches to dissect the neuronal circuitry of UPR^{ER} signaling.

Building on previous research, we were interested in understanding whether other neuronal subtypes are involved in neuron-to-body UPR^{ER} activity. We sought to determine whether glutamatergic, GABAergic, and octopaminergic neurons are necessary and/or sufficient to drive neuron-to-body communication of the UPR^{ER} in *C. elegans*. We accomplished this by overexpressing *xbp-1s* overexpression in these neuronal subtypes and assessing measurements of general health, such as lifespan, healthspan, ER function, and stress resilience. Further, we performed a comprehensive transcriptomic analysis to identify potential mechanistic pathways that drive phenotypic outcomes in these neuronal subtype UPR^{ER} paradigms.

Results

Overexpression of xbp-1s in glutamatergic, octopaminergic, and GABAergic neurons.

In previous studies, serotonergic, dopaminergic, and RIM/RIC neurons have been identified to be involved in neuron-to-body communication of UPR^{ER} [3,4]. However, these four neuron subtypes make up only ~18 of the 302 neurons in *C. elegans*, raising the question of what other neuronal subtypes may be involved in neuron-to-body UPR^{ER} communication. Previously, we performed a screen of several neurotransmitter signaling pathways involved in neuronal

communication of UPR^{ER}, which revealed glutamatergic, octopaminergic, and GABAergic neurons as candidates involved in this signaling event [3]. Glutamate is a widely utilized, excitatory neurotransmitter in both invertebrate and vertebrate systems [12]; octopamine is a *C. elegans*-specific neurotransmitter similar to the mammalian norepinephrine, and is involved in immune response [13]; and gamma-aminobutyric acid (GABA) is a widely utilized neurotransmitter that has been found to function as both an excitatory and an inhibitory signal in *C. elegans* [14]. *C. elegans* possess 79 glutamatergic neurons, 2 octopaminergic neurons, and 32 GABAergic neurons in hermaphrodites (**Fig. S1A**) (Loer CM, Worm Atlas).

To determine the potential involvement of glutamatergic, octopaminergic, and GABAergic neurons in neuron-to-body communication of UPR^{ER}, we overexpressed *xbp-1s* in each neuronal subtype using the *eat-4* promoter for *xbp-1s* overexpression in glutamatergic neurons [15] (hereafter referred to as glutamatergic *xbp-1s*); *tbh-1* promoter for *xbp-1s* overexpression in octopaminergic neurons [16] (hereafter referred to as octopaminergic *xbp-1s*); and the *unc-25* promoter for *xbp-1s* overexpression in GABAergic neurons [17] (hereafter referred to as GABAergic *xbp-1s*). We confirmed by quantitative PCR (qPCR) that all three subtypes display an increase in *xbp-1s* mRNA. Although our data did not reach statistical significance, all three neuronal *xbp-1s* subtypes did display an increase in *xbp-1s* expression (**Fig. S1B**).

***Glutamatergic, octopaminergic, and GABAergic xbp-1s alter distinct transcriptional pathways*.**

To more thoroughly investigate the impact of neuronal subtype UPR^{ER} on the periphery, we performed whole-worm RNA sequencing on animals overexpressing *xbp-1s* in glutamatergic, octopaminergic, and GABAergic neurons. Glutamatergic and octopaminergic *xbp-1s* resulted in sizable changes to gene expression, while more mild changes occurred with GABAergic *xbp-1s* (**Fig. 1A-C, Table S1**). Interestingly, the majority of differentially expressed genes were unique to each condition, suggesting distinct responses were induced by each neuronal subtype (**Fig. 1D, Table S2**). This adds more insight into a previous study that identified distinct pathways activated downstream of serotonergic and dopaminergic *xbp-1s* [3].

To further characterize the similarities and differences between peripheral response to neuronal subtype UPR^{ER}, we directly compared our glutamatergic, octopaminergic, and GABAergic *xbp-1s* animals to previously published RNA-seq datasets [3,8]. First, we sought to determine the overlap between neuronal subtype *xbp-1s* overexpression with pan-neuronal *xbp-1s* overexpression (hereafter referred to as neuronal *xbp-1s*), as we would expect that neuronal *xbp-1s* includes each neuronal subtype. We compared neuronal *xbp-1s* using two different promoters, *rab-3p* and *rgef-1p*, and were surprised to find that while there was significant overlap between these two neuronal *xbp-1s* strains, as a majority of differentially expressed genes were not shared (**Fig. S2A, Table S2**). Since this could potentially be due to leakiness of the *rab-3p* compared to the *rgef-1p* [18,19], in our subsequent studies, we focused on making comparisons to results from the *rgef-1p::xbp-1s* strain (which we will continue to refer to as neuronal *xbp-1s*).

As expected, neuronal *xbp-1s* animals display altered expression of a large number of direct XBP-1s targets [20]. Interestingly, we see that glutamatergic *xbp-1s* similarly induces many of these XBP-1s targets and to an even greater extent than neuronal *xbp-1s* (**Fig. 1E, Table S3**). These data suggest that glutamatergic *xbp-1s* activates a more canonical UPR^{ER} signature involved in conventional protein processing pathways. Gene ontology (GO) enrichment analysis supported this idea, as the most enriched biological processes included pathways related to ER function and protein homoeostasis, including ER to Golgi vesicle-mediated transport, protein N-

linked glycosylation, endoplasmic-reticulum-associated protein degradation (ERAD) pathway, and proteolysis (**Fig. 1F, Table S4**). However, a majority of differentially expressed genes in glutamatergic *xbp-1s* are still distinct from neuronal *xbp-1s* (**Fig. S2B, Table S2**), suggesting that these protein homeostatic pathways are being regulated in different ways in each condition. Interestingly, glutamatergic *xbp-1s* transcriptionally regulates an entirely different set of genes than serotonergic *xbp-1s* (**Fig. S2C, Table S2**), although these animals were also shown to induce canonical protein homeostasis pathways [3]. Altogether, these data show that even amongst neuronal subtypes that share a response (e.g., protein homeostasis), the specific genes targeted in these similar pathways are distinct, highlighting the fact that non-autonomous UPR^{ER} is dramatically different based on which neuronal subtype is involved.

Octopaminergic *xbp-1s* showed smaller gene expression changes to XBP-1s targets in comparison to glutamatergic *xbp-1s*, being more reminiscent of the levels found in neuronal *xbp-1s* (**Fig. 1E, Table S3**). However, similar to glutamatergic *xbp-1s*, when all differentially expressed genes were compared, the majority of differentially expressed genes were distinct (**Fig. S2B**). The differentially expressed genes identified were entirely different from those found in serotonergic and dopaminergic *xbp-1s* (**Fig. S2C-D, Table S2**). GO analysis identified that the most dramatic changes in gene expression in octopaminergic *xbp-1s* were defense response pathways, particularly those involved in immune response (**Fig. 1G, S2E, Table S3**). These data are consistent with previous findings that showed pathogen response in *C. elegans* is associated with UPR^{ER} induction [21] and a role for non-autonomous signaling in this response [11], potentially through octopaminergic signaling [13]. These data add an additional downstream function of non-autonomous UPRER in regulation of immune response, potentially downstream of octopaminergic neurons.

Finally, GABAergic *xbp-1s* activation caused minimal changes in gene expression overall, with very little overlap with other neuronal subtype *xbp-1s* (**Fig 1E, S2B-D**). Although the gene expression changes were minor, GO analysis did reveal some pathways previously associated with UPR^{ER} induction, including lipid remodeling [3,5] (**Fig. 1H, S2F, Table S3-4**). Altogether, our data adds more evidence to the previously proposed model [22] that specific neuronal subtypes participate in activation of unique downstream pathways in response to stress.

Glutamatergic xbp-1s promotes protein homeostasis and ER stress resilience.
To determine the physiological impact of the transcriptional changes, we next tested the ability of animals with neuronal subtype *xbp-1s* to resist specific stressors. Tunicamycin is a well-characterized ER stressor which blocks N-linked glycosylation in the ER [23], and animals with neuronal *xbp-1s* exhibit an increased resistance to tunicamycin.[2]. Consistent with our transcriptomics data, glutamatergic *xbp-1s* resulted in a small but significant increase in tunicamycin resistance (**Fig. 2A**), while octopaminergic (**Fig. 2B**) and GABAergic activation (**Fig. 2C**) had no effect on resistance to ER stress. Next, to determine whether UPR^{ER} activation in these neurons can affect proteostasis specifically in distal tissue, we crossed glutamatergic, octopaminergic, and GABAergic overexpressing *xbp-1s* strains into animals expressing fluorescently-tagged aggregation-prone polyglutamine repeats in the intestine [24] and assessed the extent of aggregation as these animals aged. Strikingly, a significant decrease in fluorescence intensity was observed at days 1 and 5 of adulthood for all three strains as compared to controls, with octopaminergic *xbp-1s* expression demonstrating the greatest reduction in fluorescence (**Fig 2D-E**). This suggests that while only glutamatergic *xbp-1s* improved ER proteotoxic stress resistance, all neuronal subtype *xbp-1s* animals have improved peripheral protein homeostasis.

***Glutamatergic, octopaminergic, and GABAergic xbp-1s* improve immune function.**

In addition to changes in protein homeostasis pathways, our transcriptomics analysis revealed that glutamatergic, octopaminergic, and GABAergic *xbp-1s* displayed significant changes in immune response related genes, with octopaminergic *xbp-1s* animals having defense response against bacteria as one of the most significantly enriched GO terms. Therefore, we measured the impact of *xbp-1s* overexpression on innate immune response using multiple methods. First, we used a standard pathogen resistance assay using exposure to *Pseudomonas aeruginosa* [25]. Using a canonical *P. aeruginosa* fast kill assay, we found that glutamatergic, octopaminergic, and GABAergic *xbp-1s* animals all displayed a significant increase in survival against PA14, with the octopaminergic *xbp-1s* displaying the most significant increase in survival even after 8 hours (**Fig. 3A**). This is consistent with the octopaminergic *xbp-1s* animals having the highest change in expression of genes associated with immune response and previous reports that indicate a functional role for octopamine signaling in innate immunity in *C. elegans* [13]. In addition, our data add further evidence that animals with improved protein homeostasis have improved immune response, as *C. elegans* innate immunity is a protein-synthesis dependent process [21].

C. elegans also utilize their nervous system for aversive learning behavior to avoid pathogenic bacteria [26]. This avoidance behavior is mediated by several neurotransmitters, including serotonin [27] and octopamine [28], and certain strains with heightened stress responses have been shown to lack this typical avoidance behavior [29]. Here, we used a previously validated forced exposure method [29] to determine the impact of neuronal *xbp-1s* overexpression on pathogen apathy. Similar to pathogen resistance, glutamatergic, octopaminergic, and GABAergic *xbp-1s* animals all displayed increased apathy to pathogens, with glutamatergic animals having the mildest phenotype (**Fig. 3B**). Thus, it is likely that the heightened resistance to pathogens is directly correlated with a lack of urgency to escape these pathogens. While we did observe an increase in expression of innate immune response genes, it is also possible that the increase in pathogen resistance is due to an increase in gut barrier integrity, as age-associated loss of gut barrier integrity results in infiltration of bacteria and bacterial colonization in the gut [30,31]. Interestingly, glutamatergic, octopaminergic, and GABAergic *xbp-1s* animals all showed similar breakdown of gut barrier integrity and age-associated bacterial colonization in the gut compared to wildtype controls, with octopaminergic *xbp-1s* animals having a trend for worse gut barrier integrity (**Fig. 3C-D**), despite having shown the highest level of resistance to pathogens (**Fig. 3A**). These data suggest that the pathogen resistance and apathy of glutamatergic, octopaminergic, and GABAergic *xbp-1s* animals is likely due to a heightened immune response, rather than a gut-barrier-related phenotype.

Glutamatergic, octopaminergic, and GABAergic xbp-1s do not alter general organismal health.

Next, we sought to test the impact of neuronal subtype *xbp-1s* on general organismal health, as previous studies have shown that neuronal *xbp-1s* results in a significant improvement in longevity and animal health, with a reduction in reproductive health [2,16]. Interestingly, we did not find any changes in general lifespan in glutamatergic, octopaminergic, or GABAergic *xbp-1s* animals (**Fig. S3**). In addition, while we saw a mild decrease in brood size in glutamatergic, octopaminergic, or GABAergic *xbp-1s* animals, these differences were not statistically significant (**Fig. S4A-C**). Finally, general organismal health was also unchanged as no change in motility was observed (**Fig. S4D-F**).

In addition to improvements in general health, neuronal *xbp-1s* animals were shown to exhibit changes in ER morphology associated with increased lysosomal function and autophagy [6,7]. These changes were associated with a general increase in secretory capacity of the ER and depletion of lipids, potentially through an increase in lipophagy [6]. Therefore, to measure general changes to the ER, we first performed imaging of the ER using an mRuby::HDEL fused to an

HSP-4 signal sequence to localize the fluorophore to the ER [6]. Since we could not successfully make homozygous octopaminergic *xbp-1s* animals with this mRuby::HDEL marker, we used an mCherry::HDEL fused to a SEL-1 signal sequence, which previous studies have shown display similar ER morphology [6]. Using these ER-localized fluorophores, we did not observe major changes to ER morphology in glutamatergic, octopaminergic, or GABAergic *xbp-1s* animals (**Fig. S5**). Next, to measure ER secretory capacity, we utilized the yolk protein marker, VIT-2::GFP. This maternal yolk protein is secreted by the intestinal ER in adults and subsequently endocytosed by developing eggs and is a commonly used marker for secretory capacity [32,33]. Although fluorescent levels appear to be higher in intact animals (**Fig. S6A**), when we quantitatively measured fluorescent levels in isolated eggs, there was no significant change in VIT-2::GFP signal (**Fig. S6B-C**), suggesting that there are no changes to ER secretory capacity in glutamatergic, octopaminergic, or GABAergic *xbp-1s* animals.

Finally, we measured lipid levels using DHS-3::GFP an abundant protein on the surface of *C. elegans* intestinal lipid droplets [34,35]. Interestingly, we saw a significant decrease in lipid droplet abundance in glutamatergic, octopaminergic, or GABAergic *xbp-1s* animals (**Fig. 4A**), despite no major changes in lipid droplet size or morphology (**Fig. 4B**). To further evaluate changes in lipid content, we utilized a more comprehensive dye, Oil Red O (ORO), which stains neutral lipids, cholesteryl esters, and lipoproteins [36]. Consistent with lipid droplet imaging, we observed a significant decrease in lipid content in glutamatergic, octopaminergic, or GABAergic *xbp-1s* animals using ORO (**Fig. 4C-D**). These data suggest that similar to other paradigms of neuronal *xbp-1s* overexpression [3,5,6], glutamatergic, octopaminergic, or GABAergic *xbp-1s* animals results in depletion of neutral lipids, likely resulting in improved lipid homeostasis.

Discussion

The UPR^{ER} is involved in diverse cellular processes that impact organismal health, including proteostasis [2,37], autophagy [7], lipid metabolism [5,6], and immune response [38]. Many of these functions can occur in a non-autonomous fashion, whereby neural cells with XBP-1s activation can coordinate a signal to the body to coordinate a homeostatic response [22]. Numerous neural circuits have been implicated in this response, including serotonin, dopamine [3], tyramine [4], RIM/RIC interneurons [11], and glial cells [8]. This study adds to this complex neural circuitry, adding additional functional roles for glutamatergic, octopaminergic, and GABAergic neurons in non-autonomous UPR^{ER} signaling.

In our current study, we overexpress *xbp-1s* in glutamatergic, octopaminergic, and GABAergic neurons, which requires several considerations. First, promoter strength and neuron number can drive different phenotypes across each neuronal *xbp-1s* overexpression paradigm, which have nothing to do with the biological significance of neuron identity. This is especially important to consider in the face of using two different neuron-specific promoters, *rab-3p* and *rgef-1p*, displaying dramatically different downstream transcriptional responses. However, our data showed that *xbp-1s* expression level alone does not purely drive phenotypic outcome. While previous studies utilizing pan-neuronal, serotonergic, or dopaminergic *xbp-1s* showed a significant increase in *xbp-1s* overexpression [3], in our study, although we can see a trend for an increase in *xbp-1s* expression in glutamatergic, octopaminergic, and GABAergic *xbp-1s*, these data did not reach statistical significance. Despite this lack of a significant increase in *xbp-1s* levels, we still saw dramatic changes in transcriptome, especially in glutamatergic and octopaminergic *xbp-1s*, with many genes implicated as canonical XBP-1s targets [39], including protein homeostasis [2] and immune response [21]. In addition, while octopaminergic neurons represent the lowest number of total neurons (2 neurons) compared to glutamatergic (79) and GABAergic (34), octopaminergic *xbp-1s* displayed some of the strongest phenotypes observed in our study. Taken together, these data argue that neuron number and promoter strength alone

do not drive phenotypic outcomes, and neuronal identity is a critical factor in non-autonomous signaling, even when using an artificial system such as *xbp-1s* overexpression.

Another potential limitation of ectopic gene overexpression is whether our findings correlate with the endogenous roles these neuronal subtypes play in signaling or gene regulation. Previous work in numerous animal models provide sufficient evidence that this is the case: in *C. elegans*, olfactory sensation of pathogenic bacteria utilize neuron-to-body XBP-1s signaling through TGF-β signaling to improve longevity and healthspan [11]. In mice, Xbp1s overexpression in POMC neurons promotes adipose tissue UPR^{ER} to improve metabolic health [9], which is very similar to hepatic *Xbp1s* activation to promote metabolic health downstream of food perception [10]. In *D. melanogaster*, glutamate signaling can promote lipid mobilization as a systemic metabolite, altering lipid metabolism [40]. These reports suggest that even ectopic genetic models can provide mechanistic insight into important endogenous physiological processes.
One interesting finding in our study is that although GABAergic *xbp-1s* had minimal changes to gene expression, these animals still displayed significant changes to organismal health, including improved proteostasis and immune response. While transcriptional changes are not the only change that could translate to physiology, as altered protein function, organelle dynamics, and metabolism can all occur in the absence of transcriptional change, technical limitations could also be responsible for the lack of difference observed in GABAergic *xbp-1s*. Here, we used whole-worm transcriptomics, and it is entirely possible that opposite changes in gene expression in different tissues could result in a net result of no change. Indeed, in terms of *xbp-1s* overexpression, this is seen where whole-body overexpression of *xbp-1s* does not result in lifespan extension, likely do to the summation of negative effects in the muscle and positive effects in the intestine and neurons [2]. Thus, it is entirely possible that GABAergic *xbp-1s* may drive differential effects in different tissue, as it does drive depletion of lipids and increased protein homeostasis in the intestine. Future tissue-specific studies can reveal whether these physiological outputs are dependent on gene expression changes in the intestine in these animals.

One final consideration is that in this study, we are generalizing neuronal signals as separate entities, although neuronal circuits are often intertwined and complex [41]. There are known neuron-neuron interactions even amongst the limited neuronal subtypes in this study. For example, dopamine and octopamine coordinate appetite regulation in crickets [42]; and excitatory glutamatergic and inhibitory GABAergic synapses strategically converge on specific cell types of the brain [43]. While our previous study has separated the utility of dopamine in serotonergic *xbp-1s* signaling and vice versa [3], this does not preclude the convergence of other neuronal subtypes. For example, we find that although glutamatergic *xbp-1s* animals display mostly changes to protein homeostasis-related pathways, they also show improved immune function and lipid depletion. While the increase in protein homeostasis could be responsible for increased immune function [21], it is entirely possible that glutamatergic neurons can also recruit octopaminergic or GABAergic signaling to alter immune response and lipid metabolism. Future studies mapping the neural circuitry across subtypes will be necessary to develop a full neural map of non-autonomous XBP-1s signaling. Overall, our study adds to the complex literature of non-autonomous XBP-1s signaling, adding three additional neuronal subtypes to this rapidly expanding map.

Materials and Methods

C. elegans maintenance

All strains utilized in this investigation are derived from the N2 wild-type worm sourced from the Caenorhabditis Genetics Center (CGC) and are detailed below. The worms are maintained at

15°C, fed with OP50 *E. coli* B strain. Animals are bleached and L1 arrested as described below for all experimentation and transferred to growth conditions at 20°C, utilizing HT115 *E. coli* K strain for all experiments. Experiments employed HT115 bacteria carrying an empty pL4440 vector referred to as empty vector (EV).

Plates

Standard NGM plates for maintenance using OP50 contained the following: Bacto-Agar (Difco) 2% w/v, Bacto Peptone 0.25% w/v, $NaCl_2$ 0.3% w/v, 1 mM $CaCl_2$, 5 µg/ml cholesterol, 0.625 mM KPO_4 pH 6.0, 1 mM $MgSO_4$.

Standard NGM plates for experimental condition using HT115 bacteria contained the following: 2% RNAi plates for experiments contained the following: Bacto-Agar (Difco) 2% w/v, Bacto Peptone 0.25% w/v, $NaCl_2$ 0.3% w/v, 1 mM $CaCl_2$, 5 µg/ml cholesterol, 0.625 mM KPO_4 pH 6.0, 1 mM $MgSO_4$, 100 µg/mL carbenicillin, 1 mM IPTG.

For all aging experiments, 100 µL of 10 mg/mL (+)-5-Fluorodeoxyuridine (FUDR) was placed directly on the bacterial lawn.

Bleaching

Experiments were conducted on animals of the same age, synchronized using a standard bleaching protocol. Worms were collected into a 15 mL conical tube using M9 solution (22 mM KH_2PO_4 monobasic, 42.3 mM $NaHPO_4$, 85.6 mM NaCl, 1 mM $MgSO_4$) and subjected to a bleaching solution (1.8% sodium hypochlorite, 0.375 M NaOH in M9) until complete digestion of carcasses. Intact eggs were then washed four times with M9 solution by centrifugation at 1.1 RCF for 30 seconds. After the final wash, animals were L1 arrested by incubating overnight in M9 at 20°C on a rotator for a maximum of 24 hours.

Transgenic strain synthesis

The sequence for *xbp-1s* expression was defined as per[2] and is provided below. Coding sequences were cloned from cDNA synthesized via reverse transcriptase using RNA isolated from N2 worms, the endogenous *eat-4p*, *tbh-1p*, and *unc-25p* promoter was cloned from gDNA isolated from N2 worms, and an *unc-54* 3′UTR was cloned from gDNA isolated from N2 worms. Plasmids were injected into N2 worms using a standard microinjection protocol as described [44] with 10 ng/µl of overexpression plasmid, 2.5 ng/µl of *myo-2p::mCherry* or *myo-2p::GFP* as a co-injection marker. Both injections and integration of constructs were performed by SUNY Biotech. All integrated animals were then backcrossed to our N2 lines to eliminate mutations and create an isogenic line. All sequences used in this manuscript are as follows:

xbp-1s

ATGAGCAACTATCCAAAACGTATTTATGTGCTCCCAGCACGCCACGTGGCAGCGCCACAG
CCTCAGAGAATGGCTCCCAAGCGTGCACTTCCAACAGAACAAGTTGTCGCACAACTTCTTG
GCGATGATATGGGACCATCTGGGCCACGCAAAAGAGAACGACTGAATCATTTGAGTCAGG
AGGAGAAAATGGATCGTCGGAAACTTAAAAATCGAGTCGCAGCCCAAAATGCTAGAGACAA
AAAGAAGGAAAGATCAGCAAAGATCGAGGATGTGATGCGCGATCTGGTGGAGGAGAACCG
CCGGCTCCGCGCTGAAAACGAACGTCTTCGCCGTCAAAATAAAAATCTTATGAACCAGCAG
AACGAGTCCGTCATGTATATGGAAGAGAACAACGAAAACTTGATGAACAGCAATGATGCAT
GCATCTACCAGAACGTCGTCTACGAAGAAGAAGTCGTCGGTGAGGTTGCACCAGTTGTCG
TCGTCGGAGGAGAGGATCGCCGTGCCTTTGAATCAGCAGTGGGAACAGGCCCGATCCAC
CTCCATCAACAACAACATCAGCAACCAACTCCGTCGTATGGATTCCAAGAAGAACAACACA
ATCAGTGTGGATATGTATCTAACTATCATCTCGATTCTATGCAACCACATGGATCGCAACAA
GAAGATGGACACCTCGAACAAATCCTCGAACATCTCAAGAGCCCAAGCGGAGAGTTCGAT

CGATTCGTTGCTGGCTACATTGAGGAAGGAGCAGACGGTTATGCAGCGTCTTGTTCAAGC
GGATCCATGTACACATCTTCAGAAACGCGTGAAACACTTTCGCCGAATTCCCTAGCCATGT
CCCCGTCGATGAGCAGCTCGAGCACTGACTGGGATGATGAGCTTTTGGGATGTGGAACCG
AAACTGGAACTGGAACCGACGAGCTGCTTACCGACCCCGGAAACTGGAACTTTGAAACTTT
CGACGAAAATTCAATCGACCTAAATTTCTTCCAAAATTAA

unc-54 UTR
CATCTCGCGCCCGTGCCTCTGACTTCTAAGTCCAATTACTCTTCAACATCCCTACATGCTCT
TTCTCCCTGTGCTCCCACCCCCTATTTTTGTTATTATCAAAAAACTTCTCTTAATTTCTTTGTT
TTTTAGCTTCTTTTAAGTCACCTCTAACAATGAAATTGTGTAGATTCAAAAATAGAATTAATT
CGTAATAAAAAGTCGAAAAAAATTGTGCTCCCTCCCCCCATTAATAATAATTCTATCCCAAA
ATCTACACAATGTTCTGTGTACACTTCTTATGTTTTTTACTTCTGATAAATTTTTTTGAAACAT
CATAGAAAAAACCGCACACAAAATACCTTATCATATGTTACGTTTCAGTTTATGACCGCAAT
TTTTATTTCTTCGCACGTCTGGGCCTCTCATGACGTCAAATCATGCTCATCGTGAAAAAGTT
TTGGAGTATTTTTGGAATTTTTCAATCAAGTGAAAGTTTATGAAATTAATTTTCCTGCTTTTG
CTTTTTGGGGTTTCCCCTATTGTTTGTCAAGATTTCGAGGACGGCGTTTTTCTTGCTAAAAT
CACAAGTATTGATGAGCACGATGCAAGAAAGATCGGAAGAAGGTTTGGGTTTGAGGCTCA
GTGGAAG

eat-4p
ATTTCTAATAAAACGGTCTACCATTTTGAGTCTATTATAGCCGAAAATCTCCAATGTGACTGT
GACTTCTTAAAACTACTAAAACATTATTTGTCCATTTACATCTTCCTAAAACCGTATATCATC
AAAAACATTCACAAAATCCGAAAAATGAGACAAAAATTTTTTTTTGATTGTTATTGCAATAAA
TCTAATAAAAATATTCATATATTGCCTGGCGCCCCCCATATCTCCATTTCCGGTCCCATCAC
CCCCACACCTCCAAGATTGATAGGTGGCTATAAGCATTTTTTGCATTTGAATGTGTTGCACC
AGTAGTCATCATCATCATTATCTAAACTGACGTGATAGTAGGGGGCTTTCTAGAAGTCGATT
TTCTATTAATGTCAACTTCATTCGTTGTCCCTTCCTTTCCCCGTCTTCCCTCACTTCCTTTTT
TCTATTTTTTCCAGTGGTCCGTAGTGGGCGGCACCCGATTTTGACTTGAAATCAGACCCGT
TTCCGGTTCTTTTGGTAGTTGTTAAGTTCTGATTCTATGACGTGGAGTGAAACAAAGAACGA
CCATATTTCATGTGTTGTGTTTTCTAGGCAGTCTAGGCAGGCAGTAGGCAGATACTGTCAA
AATTGGAATATTTCCATCTTCTAAATACCCTCAACTATTTGTTAGCGCGTTTGAAACAATAAT
TGCAAAACATTTTTTTCGCATTGATTGGGGCATTTTGAAATTTAGAGTAAAATCGACTATCAA
CTGTCATTCCATAATAATTGGCAGAATTATTTTGGTTATGCCACCAAATAATCAATAAAGAAA
GATTTCTGTCCTTATTAAACTAAAAATTGAAGCAACGGTAGAGTTGCTGAACACAGTCGCCG
GCAAAATTTTTTAATTTTCTGCAAATTTGAAATTCTTTTGCGGGTTTTTAGTTATGGTTCTAAT
AGTGGTTAAAAGTCATTATAAAACACTTCAATTTTTTGTAATGCTTTCATTCGCAGTCGTGAA
GTCGTGAAAACTCAGTTTTCACCTATCCTAACTTTGGAAGTCGTCCAAAAAATTATTTTAATT
CTACAATTTTATATTTCTTTTTAAACATACGATGTGATCAATCCTACATCAATTCTGCAAATTT
CTCACATTCTTGGAAGCTTGGTAATTTATCAGACTTTGACTGAAAATTTGAAAAAAAATTCAG
TAATTTTTGGAGATCCCTTTAAATATTATTCTAGCATTGCCATATAGAATAATTGCAAAATTC
AATTGGTTTCCTAGAAAGAAAATTAGATAATCTTATGAAAGAGAACCTAACCACAACAGGTG
TTAAATATTGATTTAAACACTAAAAAAAGTCTCTCCTTCTACCTCTCTTCTCATAGCTTTCAT
GTCTTGAAGCTTTTCGGTTAATTCGAGCGGAAGACTTATCAAGGTACGTCATTTTCAATTAC
TTGTATACATCTCTCAGCTTCTTCTAATTTTCCATGTACATCTTAGATATTCTTTTTTCAGCGA
CTTGATATTAGGAAGTTTTGTGTTTTCAATTTTAAAGTTGGATTAATATAGAATACCAGTCTT
TAAACACAAACCAACAAGGGTTCAATATCAAAATAGAAACCGAAAAAAAATATCGAAAACTG
AAAAAATCAAATACATATCTAAAGCAAGCTATTCGAGAAATATTTATGCATTATAACAACTAT
GCAGCGCTTATATCTTTATTTTTCAACAAGTGTTCCAGCAACGAGAGTCTCTTCACCAAAAA
GCCATCTATCAAAAACCAGGCAGTGAGTCCTAGAACCAAGCTTGTCAGAAGACAAGTGCAT
GTATAAATAAGTAGTAAAAGACGGGTGGGACCCAGCGCGGTGAGTAGTAGATCATAAAAAA

GTGACTGAAAAGAAGGGGCGTTTCCTTTTCTTTATTACCTCTTCCTCTACTTCTTCTCATCTC
AACTTGCTTTTTCCTTCCTCTTACAACAACTCCATCATCATCATCATCATTTTCAGAAACC

tbh-1p

GAAATGTGTGTAGTGTCATGCTCAAAATAAAATCTGGCTATAGAGGTTACAAAAAGTATGGT
TGCAATGATGTTACATAAATTGTGCCCACATGAAATTATGCAAGATAATTGGTAATGGGGTT
GCTCATGTGATGACGGAAAATGCATAAATATATTTTGTTCACTTTTCCCCTATTCATGTGTGT
AGAAGAATGTAAAAATACGCATGCATGTTTTGCATTTTTCAACATTTTTCGGCATTTTTGTAC
ATTTTTCTACATCAGCCGACAGCCCACTTCACATGCTGAAGGCGAGAAACGCAGTGAGATG
TGCCCCCGCAATGTCGAAAAATGCCGAAAAATGCAGAAACTGCATGCGTTTTTTTTACATTT
TACTACACACATGGCTAGGGGAAAAAAAAATGTAAAAATACATTTTTGCAATTTTCGTAATAA
CATAAATAACCCCATAAATGTCTTTTTTATAACTAGAATTCTAGAATTTCCTTAAAGCCACAA
AGATATTCCTCTGAAATTTTATTTTTATCTGACTGTGACTTATCTTGTTTCTATTATGTGCATT
TTTTGTCGTTAGCTTTGTCGGCTCCAAATTAAATTTCATAAATTATCAATAAATTATCATTGCA
CAAATATGTAACAGTATGCAATATTCACATTACAATTTTATTTTGATTTCTCTACTGGTAGAG
TTGATGGTTGCGTTGGTGCAGCTGCAGTAGTTCTTACATATTTTGAAGAGCGAAGAGCCTC
GGCGGATAAAAAGTAGTGTCCATTTTCTCGTCGGATACTCCGGAGCAGCGCAGTTTGATGT
ATCAGCTTCTCTGCTGGACATGTTTGAATCTAAATTTTCAGAACTTTCAAAAGAACTAACAAT
TTTCATATCCCACCAGCTTTTGACGTTTTCCAATCTCGAGCTCTTGAAACAAATTCCTATATG
TTGTTTGCGTGTCAAGCGGCACATTTGATCTGAAAAATGAAATTCTTGATAAGAATTCAATT
ATCATGGAATGCTTCATTACACTGGCAAAGCGGATGCTTTTCTCGAAAGGCGTGTTCTGGC
GACGGATGCATCAAATGGTTGATATTGGCTACGGTGGGTGGTTTCAGAATAAAAGGGGATT
TTCGGAGCATCTCCTGTTTCAGATTCAGTTATTTCTCTGAAAATAAAAACTTATCAACTTTTT
CATTTCATGTGTAAGATTTGGTGGTTATCAGGATCAATACTATAAAATCTTAAAAAAAGTAAA
TTTATTTTTATTTTTTAAATATTTCCGAAAAATAGTTTTTTGTTGAGTGGTTTTTCACAACCGC
GATGTCTCTTCATTTTATTACACAAGGTATCACTTCTTTCCTTTCTTGTGTTTTTATGACTAG
CATATTCTTTTTTTGAAAGATGTGCAGTTGACAGTTTTCAAATACTCCCTGTCATTGTCACTT
GTCATTTTCATACCTCTTCTCCCTTGCGTGCGGCACTTTCCACGTATAAGCGGCGTTGTTTG
TGGTGCGCCCGTAGA

unc-25p

TCCTACCTTTTCTATCCCACTTTTTCCCCGGAATTTTGAGATTTGACATGATTTTTCAGAGAA
TTTCGAGTTTTGAGAAAAAAAAAATCAAAAAAGCGATTTTTTGGTCAAAAGCCGAAATTTAAA
GCTAGTTTTTTTGGAAATATCGATTTTTTTTTTGAGAATTTTTCGATTTTCCAAAAAAAAAATC
GAAAGTTGTTTCCCGAAAAGCCGAAATTTTTTTTGAGATATCGAAAAATCGGAGAATTTTTC
GATGTTTCCCAGAAATACTAAAATTTTGAATTTTCCGGAAAAAAAATCGTTAAAAAATTAGTT
TCTTTTAAAGACCGAAATTTAAAGTTTTTTTTTTGGAAATATCGATTTTTTCCGAGATATCTAA
AATTGAAAGAAATTTTCGATTTTCTGAGAAAAATACGAAAAAATCGAAAAAAAAACCCAAATT
TCGGTTTTTTCGTAAAAAAAGTCGTAAAAATGTAATTTTTTTCCTGAAAAATCGGAATTTTTTA
CAAAATATCGGAAAATACTCAAAAAAAAGCTGAAAATTTCGATTTTCCGGAGAAAAAATCTTT
TTAAAAAAATATTTTTTTTTTCAGAAAATAAGAAAAGCCGAAATTTATAACTATTTCTCCGGAA
ATTCGAAATTTTTAACGAAATATCGGAATAATTTTTAGATTTTTCAAGTTTGACTTTGCGAGA
AAAAAATCGGAAAAACCTCGATTCGACGCCGAAAAATGCTCCTTTTCGAAAAGATTTTTGAA
ATTTCAGAAAATCGACATGCAAGCGCGCTCCACGGCGAAATGACAACGATGATCCACCGC
CCTCAAAAAGTTGGGTCTCGTTAGGTATTTGGCGGTAAAACTGGTAAAACTCCAGTTTTGC
CTCCAACGAGACCCAATTTTTTGGGGCGGTGGTGGAGCGCGCTTGCACAAGCTGAAAGCA
TTTTTCTGCGACTCGATAATATTTTGAAAACCTGTGTCAATTCTCGAAATTCTTTTTTTAAAAA
ATAATCCCGAGCTTCTCTCAGTCCTCCTCTATGAGGATGTTCCTTTTTTTTGGTTTTTCAATT
TTTTTTAAAATTCCAAATTTCTGTTGTGCAATTCACTTCCCCCCAAGAAATCCCAAAAATCCC
CAGTTTTCCCCAAAAATGTTCCGTTTTCATGTGATTTTTCCCCCATTTTTAAAACATTTTTTTG
ACTTTTTTTTAAAATGATTATTATTATTGTTTTCTATTTCATGGCCGGTAAATTATTTTTTTTCT

TTCTTTTTTTTTTGCTCTTTTTTTTCAAGAATTTTCGAATTGTTTGAAGGGCTGCTCATCTAATC
TTTTGTCATTTTGTTCTGATGCCATCATTTCTGAGAGGACCTTTGAAGACTCGTCACGAAAC
GGGAGGGGGGCTCAAGTGAGCATTATTATTATTATTATTGTCGCAAAAAGTTTACCCCGGG
CTCCCCCTGGCTCCCCTCTTTGAGCAAGGGTTTAAGGGCTCATTTTGATGACGAATTGCTC
ATTGGGATTATAGTCACGCCCCTCTTTTGGAGCAACTACACAACTGAGCCACAGTAATCCT
TGGGGGCGGGGTCAGTAGGACCCCCTCCGGAATAGGGAAAAGCTCAGTTCACCGCCAAA
A

Strains used in this study		
C. elegans: Bristol (N2) strain as wild type (WT)	CGC	N2
C. elegans: AGD1395: *uthIs393[vha-6p::Q40::YFP+rol-6(su1006)]*	[7]	
C. elegans: AGD1415: *pwIs23[vit-2::GFP]*	[6]	
C. elegans: AGD2192: *unc-119(ed3) III; uthSi60[vha-6p::ERss::mRuby::HDEL::unc-54 3'UTR cb-unc-119(+)] IV;*	[6]	
C. elegans: RHS10: *ldrIs[dhs-3p::dhs-3::GFP + unc-76(+)]*	This study	LIU1 6x backcross
C. elegans: RHS17: *sybIs3954[tbh-1p::xbp-1s, myo-2p::mCherry]*	This study	
C. elegans: RHS18: *sybIs3923[eat-4p::xbp-1s, myo-2p::mCherry]*	This study	
C. elegans: RHS19: *glp-4(bn2) I*	This study	SS104 6x backcross
C. elegans: RHS20: *sybIs3954[tbh-1p::xbp-1s, myo-2p::mCherry], ldrIs[dhs-3p::dhs-3::GFP + unc-76(+)]*	This study	
C. elegans: RHS21: *sybIs3954[tbh-1p::xbp-1s, myo-2p::mCherry], pwIs23[vit-2::GFP]*	This study	
C. elegans: RHS57: *sybIs3970[unc-25p::xbp-1s, myo-2p::GFP]*	This study	
C. elegans: RHS59: *sybIs3970[unc-25p::xbp-1s, myo-2p::GFP]; ldrIs1[dhs-3p::dhs-3::GFP + unc-76(+)]*	This study	
C. elegans: RHS60: *sybIs3970[unc-25p::xbp-1s, myo-2p::GFP]; uthSi60[vha-6p::ERss::mRuby::HDEL::unc-54 3'UTR cb-unc-119(+)] IV;*	This study	
C. elegans: RHS62: *sybIs3970[unc-25p::xbp-1s, myo-2p::GFP]; pwIs23[vit-2::GFP]*	This study	
C. elegans: RHS74: *sybIs3923[eat-4p::xbp-1s, myo-2p::mCherry]; pwIs23[vit-2::GFP]*	This study	
C. elegans: RHS79: *sybIs3923[eat-4p::xbp-1s, myo-2p::mCherry]; ldrIs1[dhs-3p::dhs-3::GFP + unc-76(+)]*	This study	
C. elegans: RHS84: *sybIs3923[eat-4p::xbp-1s, myo-2p::mCherry]; uthSi60[vha-6p::ERss::mRuby::HDEL::unc-54 3'UTR, cb-unc-119(+)] IV*	This study	

C. elegans: RHS96: *sybIs3970[unc-25p::xbp-1s, myo-2p::GFP]; glp-4(bn2) I*	This study	
C. elegans: RHS98: *sybIs3923[eat-4p::xbp-1s, myo-2p::mCherry]; glp-4(bn2) I;*	This study	
C. elegans: RHS109: *uthIs393[vha-6p::Q40::YFP+rol-6(su1006)]; sybIs3923[eat-4p::xbp-1s, myo-2p::mCherry];*	This study	
C. elegans: RHS110: *uthIs393[vha-6p::Q40::YFP+rol-6(su1006)]; sybIs3970[unc-25p::xbp-1s, myo-2p::GFP]*	This study	
C. elegans: RHS114: *sybIs3954[tbh-1p::xbp-1s, myo-2p::mCherry]; hjSi158[vha-6p::SEL-1(1-79)::mCherry::HDEL::let-858 3' UTR]*	This study	
C. elegans: RHS133: *uthIs393[vha-6p::Q40::YFP+rol-6(su1006)]; sybIs3954[tbh-1p::xbp-1s, myo-2p::mCherry]*	This study	
C. elegans: *sybIs3954[tbh-1p::xbp-1s, myo-2p::mCherry]; glp-4(bn2) I*	This study	

Neuron Count

Worm Atlas (https://www.wormatlas.org/neurotransmitterstable.htm) summarizes the proposed neuron location for glutamatergic, octopaminergic, and GABAergic neurons in hermaphrodites.

Neuron Type	Proposed Number	Location by Body Region
Glutamatergic	79	Head: ADA, ADL, AFD, AIB, AIM, AIZ, ASE, ASG, ASH, ASK, AQR, AUA, AWC, BAG, FLP, IL1, OLL, OLQ, RIA, RIG, RIM, URY Pharynx: M3, M1, I2, I5 Ventral nerve cord and body: ALM, AVM, CP0, CP5, CP6, CP7 Tail: DVC, LUA, PHA, PHB, PHC, PLM, PVD, PVQ, PQR, PVR
Octopaminergic	2	Head: RIC
GABAergic	32	Head: AVl, DD1-6, DVB, RIB, RIS, RME, SMDD/V, VD1-13 Ventral nerve cord and body: DD2-4, VD3-11 Tail: DD6, DVB, VD12-13

***C. elegans* microscopy**

Stereoscope

For whole-worm imaging of *vha-6p::Q40::YFP*, DHS-3::GFP, and VIT-2::GFP strains, synchronized animals were grown on RNAi plates plated with HT115 empty pL4440 vector from L1 stage. Animals were imaged at day 1 of adulthood and for aging experiments also imaged at day 5 and day 9 of adulthood. 10+ animals were placed in a pool of 100 mM sodium azide in M9 on standard NGM plates without bacteria to induce paralysis. Paralyzed animals were then lined alongside each other and imaged on a Leica M205FCA automated fluorescent

stereomicroscope running LAS X software and equipped with a standard GFP filter, Leica LED3 light source, and Leica K5 camera. For all imaging experiments, 3 biological replicates were performed with 2 technical replicates each, and 1 representative image was chosen for use in figures. For *vha-6p::Q40::YFP* quantification, Fiji [45] was used to draw a region of interest along the posterior half of each group of worms, and integrated density was measured. Graphing and statistical analysis was performed with GraphPad Prism 10 software using a Mann-Whitney test.

Widefield and confocal imaging
Widefield imaging utilized a Leica THUNDER Imager equipped with a 63x/1.4 Plan AproChromat objective, standard dsRed filter (11525309), Leica DFC9000 GT camera, a Leica LED5 light source, and run on LAS X software. For high resolution imaging of DHS-3::GFP and ER morphology, imaging was performed using a Leica Stellaris 5 confocal microscope equipped with a white light laser source and spectral filters, HyD detectors, 63x/1.4 Plan ApoChromat objective, and run on LAS X software. Animals were placed in 100 mM sodium azide solution on a glass slide to induce paralysis and imaged within 5 minutes of slide preparation to prevent artifacts from prolonged exposure to sodium azide. For all imaging experiments, 3 biological replicates were performed with 2 technical replicates each, and 1 representative image was chosen for use in figures.

Intestinal bacteria invasion assay
Assessing intestinal bacteria invasion was performed as previously described [46]. Animals were L1 synchronized via bleaching and plated on RNAi plates containing a bacterial lawn derived from a mixture of 80% HT115 bacteria containing empty pL4440 vector and 20% HT115 bacteria expressing mCherry. Once at the desired age, animals were manually transferred onto a standard OP50 plate and allowed to feed on OP50 for 2 hours at 20°C to facilitate clearance of mCherry bacteria. For imaging, worms were paralyzed by exposure to M9 solution containing 100 mM sodium azide and arranged on a standard NGM plate without bacteria. Images were captured using a Leica M205FCA fluorescent stereomicroscope equipped with a standard dsRed filter as described above. For each of the 3 biological replicates, 2 technical replicates with 13 animals per replicate were performed and 1 representative image was used for figures. The percentage of animals exhibiting bacterial invasion was quantified and plotted with GraphPad Prism 10 software for each technical and biological replicate. Statistical analysis was conducted across all replicates using a Mann-Whitney test with GraphPad Prism 10 software.

ER Secretion Assay
Assaying of ER secretory function was performed as described previously [47]. Transgenic control animals and *eat-4p::xbp-1s*, *tbh-1p::xbp-1s*, and *unc-25p::xbp-1s* animals expressing VIT-2::GFP were bleached to obtain eggs. Eggs were then placed on glass slides and imaged using a Leica THUNDER Imager equipped with a 63x/1.4 Plan AproChromat objective, standard dsRed filter (11525309), Leica DFC9000 GT camera, a Leica LED5 light source, and run on LAS X software. Images were quantified using Fiji and drawing a region of interest around each individual egg to obtain an integrated density value. 4 independent biological replicates were performed. SuperPlots [48] were created using GraphPad Prism 10 software where large dots represent the median value of each biological replicate and small dots represent single eggs with different intensities of colors representing eggs from the same biological replicate; lines indicate median and interquartile range. All statistical analyses were conducted using Mann–Whitney testing with GraphPad Prism 10 software. For whole worm imaging, animals were raised to day 3 of adulthood and imaged using the Leica M205FCA fluorescent stereomicroscope equipped with a standard GFP filter as described above.

Oil Red O Staining

Oil Red O fat staining was performed as previously described [49]. Briefly, worms were bleached, and eggs were plated to obtain a synchronous population. Worms were grown on RNAi plates with a lawn of HT115 bacteria containing an empty pL4440 vector and aged to day 3 of adulthood or day 5 of adulthood. Aging was performed in the absence of FUDR by gravity settling in M9 solution and aspirating to remove progeny. For staining, worms were washed off plates using a PBS + 0.01% Triton solution, rocked for 3 minutes in 40% isopropyl alcohol, pelleted, and then stained with Oil Red O in diH_2O for 2 hours while rocking at room temperature. Worms were pelleted and washed in PBS + 0.01% Triton for 30 min before being imaged at 20× magnification with a Leica THUNDER Imager Flexacam C3 color camera and run on LAS X software. To quantify somatic fat depletion, worms were scored as previously described [50]. The level and distribution of fat was placed into categories of non-somatic lipid depletion, displaying no loss of fat and being darkly stained throughout the body, and somatic lipid depletion, being stained largely in the germ cells. At least 100 worms were scored for each condition over 3 biological replicates.

***Caenorhabditis elegans* RT-qPCR and RNA-seq analysis**

For collection of RNA, we used *glp-4(bn2)* animals to eliminate progeny. After bleaching L1 arresting, all animals were raised at 22°C (the restrictive temperature for our backcrossed *glp-4(bn2)* strain) for 3 days to collect animals at day 1 of adulthood. Approximately 1000 animals were used per condition. Worms were collected using M9 and transferred to TRIzol solution and underwent 3 freeze/thaw cycles between liquid nitrogen and a 37°C bead bath with a 30-second vortexing step between each cycle to lyse worms. Following the final thaw, chloroform was added at a ratio of 1:5 chloroform/TRIzol, and aqueous separation of RNA was achieved by centrifugation using a heavy gel phase-lock tube (VWR, 10847–802). The aqueous phase was mixed with isopropanol at a 1:1 ratio and applied to a QuantaBio Extracta Plus RNA kit (95214) for RNA purification according to the manufacturer's instructions.

Library preparation and sequencing was conducted at Novogene using their standard pipeline using paired-end, polyA selection, first-strand synthesis, and an Illumina NovaSeq6000. Each condition was measured with 3 biological replicates. Gene expression levels were quantified using kallisto [51] with WBcel235 as the reference genome. Fold changes were determined using DESeq2 [52]. Gene targets of XBP-1 were defined based on previous experimental findings [53]. Gene Ontology (GO) enrichment analysis was performed using WormEnrichr [54,55]. *rgef-1p*, *dat-1p*, *tph-1p*, *eat-4p*, *tbh-1p*, and *unc-25p* driven expression of *xbp-1s* was compared to the N2 wild-type control.

For RT-qPCR, cDNA synthesis was conducted using qScript cDNA SuperMix (QuantaBio, 101414-102) with 500 ng of RNA. RT-qPCR was performed using NEB Q5 DNA polymerase following the manufacturer's guidelines and utilizing the primers listed below. Each condition was assessed using 3 biological replicates. QuantStudio 3 (Thermo Fisher) was used for quantification using a standard curve method.

Primer Name	Primer Sequence	Primer Purpose
xbp-1s RT-qPCR Forward	CGTGCCTTTGAATCAGCAGTG	Measurement of xbp-1s transcripts
xbp-1s RT-qPCR Reverse	CGAGGTGTCCATCTTCTTGTT	Measurement of xbp-1s transcripts
Y45F10D.4 RT-qPCR Forward	AAGCGTCGGAACAGGAATC	Housekeeping gene

Y45F10D.4 RT-qPCR Reverse	TTTTTCCGTTATCGTCGACTC	Housekeeping gene
sap-49 RT-qPCR Forward	TGGCGGATCGTCGTGCTTCC	Housekeeping gene
sap-49 RT-qPCR Reverse	ACGAGTCTCCTCGTTCGTCCCA	Housekeeping gene

Lifespan measurements

For lifespan experiments, animals were grown on RNAi plates on either EV or RNAi bacteria from L1 stage. At day 1 of adulthood, animals were washed off plates with M9 solution and then moved to plates containing 100 µL of 100 mg/mL FUDR to eliminate progeny. One replicate of lifespan assays was performed using a lifespan machine [56] with others being done by hand. Tunicamycin and thermotolerance lifespan assays were performed based on established protocols [57]. For tunicamycin assays, animals were moved onto plates supplemented with 25 µg/mL tunicamycin in DMSO directly in the plate. Animals were grown at 20°C and checked every 2 days for viability. For thermotolerance assays, day 1 adult animals were placed at 34°C and scored for viability every 2 hours. Animals were considered dead if they did not exhibit any movement when prodded with a platinum wire at both the head and the tail. Animals that exhibited bagging, intestinal leakage, desiccation on the side of the plate, or other deaths unrelated to aging were scored as censored. All lifespans were performed on 3 biological replicates. Lifespan assay survival curves were plotted using GraphPad Prism 10 software and statistics were performed using a Log-Rank test in GraphPad Prism 10. Representative data are depicted in figures and a table of all lifespan assays performed is available in **Table S5**.

***Caenorhabditis elegans* brood size assay**

Brood assays were measured as previously described [57]. Bleaching was used to obtain a synchronized population of animals, and 10 L4 stage animals were transferred onto individual plates. Every 12 hours, the animals were moved onto new plates, while plates containing eggs were stored in a 15°C incubator for 2–3 days. All surviving progeny on each egg-laying plate were counted and totaled to determine the brood size. SuperPlots [48] were created using GraphPad Prism 10 software where large dots represent the median value of each biological replicate and small dots represent single animals with different intensities of colors representing animals from the same biological replicate; lines indicate median and interquartile range. All statistical analyses were conducted using Mann–Whitney testing with GraphPad Prism 10 software.

***Caenorhabditis elegans* thrashing assay**

Thrashing assays were conducted on animals synchronized via bleaching and aged on RNAi plates containing FUDR from day 1 of adulthood. Upon reaching the desired age, plates containing adult animals were flooded with 100 µL of M9 solution, and 30-second videos were recorded using an M205FCA stereomicroscope equipped with a Leica K5 microscope running LAS X software. Thrashing movements were manually recorded over a 10 second period. A bending of more than 50% of the animal's body in the opposite direction was deemed a single thrash. Representative data from 3 independent biological replicates are presented. SuperPlots [48] were created using GraphPad Prism 10 software where large dots represent the median value of each biological replicate and small dots represent single animals with different intensities of colors representing animals from the same biological replicate; lines indicate median and interquartile range. All statistical analyses were conducted using Mann–Whitney testing with GraphPad Prism 10 software.

Fast kill assay
Fast kill assays were performed as previously described with minor modifications [58,59]. *Pseudomonas aeruginosa* (PA14) cultures were grown overnight at 37°C for 14-15 hours. 5 µL of overnight culture was spread over 3.5 cm peptone glucose media plates (1% Bacto-Peptone, 1% NaCl, 1% glucose, 1.7% Bacto Agar) containing 0.15 M sorbitol, using a spreader made from an open loop tipped glass pasture pipette. The plates were incubated at 37°C for 24 hours and then at 25°C for 48 hours. Following this, 30 to 40 synchronized L4 animals were placed on each plate. Assays were performed at 25°C. Survival of animals was plotted over a period of 8 hours with intervals of 2 hours. An animal was deemed dead when it no longer responded to touch. 3 biological replicates with 3 technical replicates were performed for a total of 9 replicates. Survival rates were measured wherein 100% survival was indicated as an integer "1" and the fraction of survival populations at every time point was represented as decimal values.

Forced food choice
Forced food choice assays were performed as described previously [29,60]. Plates were made using the same recipe for NGM plates aside from the addition of 0.35% peptone. A single colony of *Pseudomonas aeruginosa* (PA14) and *E. coli* OP50 bacteria were inoculated into separate 3 mL of LB for overnight primary culture at 37°C. The following day, the OD_{600} of each of the cultures was diluted to an OD_{600} of 1.0. A culture of PA14 was transferred as a line along the center of an NGM plate using a glass Pasteur pipette bent at a 90-degree angle. Next, 15 µL of OP50 culture was seeded as a dot onto the plate 2.5 cm away from the center and 0.5 cm away from the edge of the plate. The plates were dried and transferred to 37°C for 24 hours, followed by incubation at 25°C for 48 hours. On the day of the assay, the plates were removed from the 25°C incubator and allowed to reach room temperature. Worms were washed three times in M9 solution before being placed onto the assay plate diametrically opposite to the OP50 dot at 2.5 cm away from the center. The proportion of worms found on or off each food was recorded after 1 hour, 2 hours, 4 hours, 6 hours, and 8 hours. After each time point, the population was scored in which -1 represented 100% of the population on PA14 and +1 represented 100% of the population on OP50. The movement index was then calculated towards the OP50 dot using the formula:

("A" population of worm on OP50 dot – "B" population of worms on PA14 line)
("A" population of worm on OP50 dot + "B" population of worms on PA14 line)
Each assay was done in biological triplicate with technical triplicates for a total of 9 replicates. Statistical analyses were conducted using Mann–Whitney testing with GraphPad Prism 10 software.

Competing Financial Interests
All authors of the manuscript declare that they have no competing interests.

Data Availability
All data required to evaluate the conclusions in this manuscript are available within the manuscript and Supporting Information. All strains synthesized in this manuscript are derivatives of N2 or other strains from CGC and are either made available on CGC or available upon request. All raw RNA-seq datasets are available through Annotare 2.0 Array Express Accession E-MTAB-14132.

Acknowledgements
A.H., M.A., and G.G. are supported by T32AG052374; S.P.C. is supported by NIH R01AG058610 and Hevolution Foundation award 748 HF AGE-004; B.A.B. is supported by the Simons Collaboration on Plasticity in the Aging Brain grant SF811217; P.J.M. is supported by the Impetus Grants 014746-00001 and the Baxter award; and R.H.S. is supported by R00AG065200 and R01AG079806 from the National Institute on Aging and the Glenn

Foundation for Medical Research and AFAR Grant for Junior Faculty Award. Some strains were provided by the CGC, which is funded by the NIH Office of Research Infrastructure Programs (P40 OD010440). Some gene analysis was performed using Wormbase, which is funded on a U41 grant HG002223.

Figure Legends

Fig. 1. Glutamatergic, octopaminergic, and GABAergic *xbp-1s* modulate distinct transcriptional pathways. Volcano plots of whole-body genome-wide changes in gene expression upon *xbp-1s* overexpression in **(A)** glutamatergic, **(B)** octopaminergic, and **(C)** GABAergic neurons. Red dots indicate significantly differentially expressed genes with p-value ≤ 0.01. See **Table S1**. **(D)** Comparison of differentially expressed genes (p-value ≤ 0.01) between worms expressing *xbp-1s* in glutamatergic, octopaminergic, and GABAergic neurons. for a complete list of differentially expressed genes. See **Table S2**. **(E)** Heat map of XBP-1s target gene [20] expression under neuronal, glutamatergic, octopaminergic, and GABAergic *xbp-1s*. Warmer colors indicate increased expression, and cooler colors indicate decreased expression. See **Table S3**. Top ten most enriched gene ontology terms of differentially expressed genes upon *xbp-1s* overexpression in **(F)** glutamatergic, **(G)** octopaminergic, and **(H)** GABAergic neurons. See **Table S4**.

Fig. 2. Glutamatergic, octopaminergic, and GABAergic *xbp-1s* enhance proteostasis. (A) Survival curve of glutamatergic, octopaminergic, and GABAergic *xbp-1s* animals grown on 25 µg/mL tunicamycin starting from day 1 of adulthood. Lifespans were scored every 2 days. Data is representative of 3 replicates and statistical analysis is available in **Table S5**. **(B)** Representative images of protein aggregation in animals expressing intestinal polyglutamine repeats (*vha-6p::polyQ::YFP*) [61] in glutamatergic, octopaminergic, or GABAergic *xbp-1s* animals. All animals were imaged on day 1, 5, and 9 of adulthood. Images were captured using a Leica M205 stereo microscope. **(C)** Quantification of fluorescence integrated density (B) was performed across 2 technical replicates each of 3 biological replicates for a total of 6 replicates. Lines represent mean and standard deviation. * = $p \leq 0.05$, ** = $p \leq 0.01$, ns = $p > 0.05$ using a Mann-Whitney test.

Fig. 3. Glutamatergic, octopaminergic, and GABAergic *xbp-1s* enhance pathogen resistance and increases pathogen apathy. (A) Survival analysis of control (N2, blue), glutamatergic *xbp-1s* (green, *eat-4p*), octopaminergic *xbp-1s* (yellow, *tbh-1p*), or GABAergic *xpb-1s* (pink, *unc-25p*) on PA14 fast kill assay plates for 2, 4, 6, and 8 hours. Each fast kill assay is comprised of 3 technical replicates per biological replicate and at least 3 biological replicates per condition. Results were analyzed via two-way ANOVA test; **($p<0.01$) ***($p<0.001$) ****($p<0.0001$). **(B)** Pathogen avoidance behavior of control (N2, blue), glutamatergic *xbp-1s* (green, *eat-4p*), octopaminergic *xbp-1s* (yellow, *tbh-1p*), or GABAergic *xpb-1s* (pink, *unc-25p*) during "forced" food choice assays measured at 1, 2, 3, 6, and 8 hour time points. Each forced food choice assay is comprised of 3 technical replicates per biological replicate and at least 3 biological replicates per condition. Results were analyzed via two-way ANOVA test; **($p<0.01$) ***($p<0.001$) ****($p<0.0001$). **(C)** Representative brightfield and fluorescent images of adult worms grown on bacteria expressing mCherry. Animals are moved to OP50 plates for two hours to remove mCherry expressing bacteria from the intestine before imaging. Any remaining mCherry signal after OP50 clarification are signs of bacterial colonization. **(D)** Quantification of the percent of animals displaying intestinal bacterial colonization was performed across 2 technical replicates for each of 3 biological replicates for a total of 6 replicates. Lines represent mean and standard deviation. * = $p \leq 0.05$, ** = $p \leq 0.01$, ns = $p > 0.05$ using a Mann-Whitney test.

Fig. 4. Glutamatergic, octopaminergic, and GABAergic *xbp-1s* results in depletion of lipids. Representative fluorescent micrographs of day 3 adult animals of control, glutamatergic *xbp-1s* (*eat-4p*), octopaminergic *xbp-1s* (*tbh-1p*), and dopaminergic *xpb-1s* (*unc-25p*) taken on a stereomicroscope **(A)** and on a confocal microscope **(B).** All images are contrast matched.

Scale bar represents 10 um. **(B)** Representative images of day 3 adult animals of control, glutamatergic *xbp-1s* (*eat-4p*), octopaminergic *xbp-1s* (*tbh-1p*), and dopaminergic *xpb-1s* (*unc-25p*) of ORO-stained lipids. **(D)** Quantification of lipid staining as non-lipid depletion (black) and lipid depletion (gray).

Supplemental Figure Legends

Fig. S1. *xbp-1s* overexpression in *C. elegans* glutamatergic, octopaminergic, and dopaminergic neurons. (A) Schematic of each neuronal type explored in this study: glutamatergic, *eat-4p* (n = 79, location = head, pharynx, ventral nerve cord and body, tail), octopaminergic, *tbh-1p* (n = 2, location = head), GABAergic, *unc-25p* (n = 32, location = head, ventral nerve cord and body, tail). **(B)** qPCR of transcripts of control (blue), glutamatergic *xbp-1s* (green), octopaminergic *xbp-1s* (yellow), and GABAergic *xbp-1s* (pink) animals grown on empty vector from hatch. RNA was isolated in day 1 adults and data is compared using a standard curve with data represented as relative fold change against control. Each dot represents a biological replicate averaged across three technical replicates per sample. Lines represent geometric mean with geometric standard deviations.

Fig S2. (A) Comparison of differentially expressed genes (p-value ≤ 0.01) in neuronal *xbp-1s* driven by *rgef-1p* or *rab-3p*. Comparison of differentially expressed genes (p-value ≤ 0.01) in glutamatergic, octopaminergic, GABAergic *xbp-1s* and **(B)** neuronal *xbp-1s* driven by *rgef-1p*, **(C)** serotonergic *xbp-1s* driven by *tph-1p*, and **(D)** dopaminergic *xbp-1s* driven by *dat-1p*. See **Table S1**. Heat map of **(E)** lipid homeostasis (GO:0055088) or **(F)** immune response (GO:0006955) gene expression under pan-neuronal, glutamatergic, octopaminergic, and GABAergic *xbp-1s* overexpression. Warmer colors indicate increased expression, and cooler colors indicate decreased expression. See **Table S3**.

Fig. S3. Glutamatergic, octopaminergic, and GABAergic *xbp-1s* does not extend lifespan. Lifespan measurements of control (blue) and **(A)** glutamatergic *xbp-1s* (green, *eat-4p*), **(B)** octopaminergic *xbp-1s* (yellow, *tbh-1p*), **(C)** and GABAergic *xbp-1s* (pink, *unc-25p*) animals. Lifespans were scored every 2 days and data is representative of 3 biological replicates. All statistical analysis is available in **Table S5**.

Fig. S4. Glutamatergic, octopaminergic, and GABAergic *xbp-1s* does not increase healthspan. Measurements of fecundity of control (blue) and **(A)** glutamatergic *xbp-1s* (green, *eat-4p*), **(B)** octopaminergic *xbp-1s* (yellow, *tbh-1p*), and **(C)** GABAergic *xbp-1s* (pink, *unc-25p*) animals. Total number of eggs that hatched were counted per animal. Measurements of thrashing of control (blue) and **(D)** glutamatergic *xbp-1s* (green, *eat-4p*), **(E)** octopaminergic *xbp-1s* (yellow, *tbh-1p*), and **(F)** GABAergic *xbp-1s* (pink, *unc-25p*) animals. Number of thrashes was assessed over a 10 second period in animals at day 1 adult (young), day 4-5 adult (middle), and day 9 adult (old) in M9 solution with each thrash being counted as a movement from a concave to a convex formation. For SuperPlots, each small dot represents a single animal with various intensities of colors representing independent biological replicates and each large dot is the median value of each biological replicate. Lines represent the median across all biological replicates and whiskers indicate interquartile range. Statistical analysis was performed using a Mann-Whitney test.

Fig. S5. Glutamatergic, octopaminergic, and GABAergic *xbp-1s* does not alter ER morphology. (A) Representative fluorescent micrographs of day 3 adult mRuby::HDEL of control, glutamatergic *xbp-1s* (*eat-4p*), and GABAergic *xbp-1s* (*unc-25p*), animals. Images are representative of three independent biological replicates and are independently contrast enhanced for each individual image. Scale bar represents 10 µm. **(B)** Representative fluorescent micrographs of day 3 adult mCherry::HDEL of control and octopaminergic *xbp-1s* (*tbh-1p*), animals. Images are representative of three independent biological replicates and are independently contrast enhanced for each individual image. Scale bar represents 10 µm.

Fig. S6. Glutamatergic, octopaminergic, and GABAergic *xbp-1s* does not alter ER secretory capacity. (A) Representative fluorescent micrographs of day 3 adult animals of VIT2::GFP in control, glutamatergic *xbp-1s* (*eat-4p*), octopaminergic *xbp-1s* (*tbh-1p*), or GABAergic *xpb-1s* (*unc-25p*). All images are contrast matched. **(B)** Representative fluorescent micrographs of eggs collected using a standard bleaching protocol of day 3 adult animals of VIT2::GFP in control, glutamatergic *xbp-1s* (*eat-4p*), octopaminergic *xbp-1s* (*tbh-1p*), or GABAergic *xpb-1s* (*unc-25p*). All images are contrast matched. Scale bar represents 500 µm. **(C)** Quantification of eggs from (B) using measurements of integrated intensity. For SuperPlots, each small dot represents a single animal with various intensities of colors representing independent biological replicates and each large dot is the median value of each biological replicate. Lines represent the median across all biological replicates and whiskers indicate interquartile range. Statistical analysis was performed using a Mann-Whitney test.

Supplementary Tables:

Table S1. List of DEGs.
Table S2. Venn Diagram Gene Names.
Table S3. Heat Maps.
Table S4. GO Biological Process.
Table S5. Lifespan Statistics.

References Cited

1. Dutta, N., Garcia, G., and Higuchi-Sanabria, R. (2022). Hijacking Cellular Stress Responses to Promote Lifespan. Front. Aging *3*, 860404. https://doi.org/10.3389/fragi.2022.860404.

2. Taylor, R.C., and Dillin, A. (2013). XBP-1 Is a Cell-Nonautonomous Regulator of Stress Resistance and Longevity. Cell *153*, 1435–1447. https://doi.org/10.1016/j.cell.2013.05.042.

3. Higuchi-Sanabria, R., Durieux, J., Kelet, N., Homentcovschi, S., De Los Rios Rogers, M., Monshietehadi, S., Garcia, G., Dallarda, S., Daniele, J.R., Ramachandran, V., et al. (2020). Divergent Nodes of Non-autonomous UPRER Signaling through Serotonergic and Dopaminergic Neurons. Cell Reports *33*, 108489. https://doi.org/10.1016/j.celrep.2020.108489.

4. Özbey, N.P., Imanikia, S., Krueger, C., Hardege, I., Morud, J., Sheng, M., Schafer, W.R., Casanueva, M.O., and Taylor, R.C. (2020). Tyramine Acts Downstream of Neuronal XBP-1s to Coordinate Inter-tissue UPRER Activation and Behavior in C. elegans. Developmental Cell *55*, 754-770.e6. https://doi.org/10.1016/j.devcel.2020.10.024.

5. Imanikia, S., Sheng, M., Castro, C., Griffin, J.L., and Taylor, R.C. (2019). XBP-1 Remodels Lipid Metabolism to Extend Longevity. Cell Reports *28*, 581-589.e4. https://doi.org/10.1016/j.celrep.2019.06.057.

6. Daniele, J.R., Higuchi-Sanabria, R., Durieux, J., Monshietehadi, S., Ramachandran, V., Tronnes, S.U., Kelet, N., Sanchez, M., Metcalf, M.G., Garcia, G., et al. (2020). UPRER promotes lipophagy independent of chaperones to extend life span. Science Advances *6*, eaaz1441. https://doi.org/10.1126/sciadv.aaz1441.

7. Imanikia, S., Özbey, N.P., Krueger, C., Casanueva, M.O., and Taylor, R.C. (2019). Neuronal XBP-1 Activates Intestinal Lysosomes to Improve Proteostasis in C. elegans. Current Biology *29*, 2322-2338.e7. https://doi.org/10.1016/j.cub.2019.06.031.

8. Frakes, A.E., Metcalf, M.G., Tronnes, S.U., Bar-Ziv, R., Durieux, J., Gildea, H.K., Kandahari, N., Monshietehadi, S., and Dillin, A. (2020). Four glial cells regulate ER stress resistance and longevity via neuropeptide signaling in C. elegans. Science *367*, 436–440. https://doi.org/10.1126/science.aaz6896.

9. Williams, K.W., Liu, T., Kong, X., Fukuda, M., Deng, Y., Berglund, E.D., Deng, Z., Gao, Y., Liu, T., Sohn, J.-W., et al. (2014). Xbp1s in Pomc Neurons Connects ER Stress with Energy Balance and Glucose Homeostasis. Cell Metabolism *20*, 471–482. https://doi.org/10.1016/j.cmet.2014.06.002.

10. Brandt, C., Nolte, H., Henschke, S., Engström Ruud, L., Awazawa, M., Morgan, D.A., Gabel, P., Sprenger, H.-G., Hess, M.E., Günther, S., et al. (2018). Food Perception Primes Hepatic ER Homeostasis via Melanocortin-Dependent Control of mTOR Activation. Cell *175*, 1321-1335.e20. https://doi.org/10.1016/j.cell.2018.10.015.

11. De-Souza, E.A., Thompson, M.A., and Taylor, R.C. (2023). Olfactory chemosensation extends lifespan through TGF-β signaling and UPR activation. Nat Aging *3*, 938–947. https://doi.org/10.1038/s43587-023-00467-1.

12. Serrano-Saiz, E., Poole, R.J., Felton, T., Zhang, F., De La Cruz, E.D., and Hobert, O. (2013). Modular Control of Glutamatergic Neuronal Identity in C. elegans by Distinct Homeodomain Proteins. Cell *155*, 659–673. https://doi.org/10.1016/j.cell.2013.09.052.

13. Sellegounder, D., Yuan, C.-H., Wibisono, P., Liu, Y., and Sun, J. (2018). Octopaminergic Signaling Mediates Neural Regulation of Innate Immunity in Caenorhabditis elegans. mBio *9*, e01645-18. https://doi.org/10.1128/mBio.01645-18.

14. McIntire, S.L., Jorgensen, E., and Horvitz, H.R. (1993). Genes required for GABA function in Caenorhabditis elegans. Nature *364*, 334–337. https://doi.org/10.1038/364334a0.

15. Lee, R.Y.N., Sawin, E.R., Chalfie, M., Horvitz, H.R., and Avery, L. (1999). EAT-4, a Homolog of a Mammalian Sodium-Dependent Inorganic Phosphate Cotransporter, Is Necessary for Glutamatergic Neurotransmission in Caenorhabditis elegans. J Neurosci *19*, 159–167. https://doi.org/10.1523/JNEUROSCI.19-01-00159.1999.

16. Alkema, M.J., Hunter-Ensor, M., Ringstad, N., and Horvitz, H.R. (2005). Tyramine Functions Independently of Octopamine in the Caenorhabditis elegans Nervous System. Neuron *46*, 247–260. https://doi.org/10.1016/j.neuron.2005.02.024.

17. Jin, Y., Jorgensen, E., Hartwieg, E., and Horvitz, H.R. (1999). The Caenorhabditis elegans Gene unc-25Encodes Glutamic Acid Decarboxylase and Is Required for Synaptic Transmission But Not Synaptic Development. J Neurosci *19*, 539–548. https://doi.org/10.1523/JNEUROSCI.19-02-00539.1999.

18. Gelino, S., Chang, J.T., Kumsta, C., She, X., Davis, A., Nguyen, C., Panowski, S., and Hansen, M. (2016). Intestinal Autophagy Improves Healthspan and Longevity in C. elegans during Dietary Restriction. PLoS Genet *12*, e1006135. https://doi.org/10.1371/journal.pgen.1006135.

19. Yang, Y., Arnold, M.L., Lange, C.M., Sun, L.-H., Broussalian, M., Doroodian, S., Ebata, H., Choy, E.H., Poon, K., Moreno, T.M., et al. (2024). Autophagy protein ATG-16.2 and its WD40 domain mediate the beneficial effects of inhibiting early-acting autophagy genes in C. elegans neurons. Nat Aging *4*, 198–212. https://doi.org/10.1038/s43587-023-00548-1.

20. Urano, F., Calfon, M., Yoneda, T., Yun, C., Kiraly, M., Clark, S.G., and Ron, D. (2002). A survival pathway for Caenorhabditis elegans with a blocked unfolded protein response. Journal of Cell Biology *158*, 639–646. https://doi.org/10.1083/jcb.200203086.

21. Richardson, C.E., Kooistra, T., and Kim, D.H. (2010). An essential role for XBP-1 in host protection against immune activation in C. elegans. Nature *463*, 1092–1095. https://doi.org/10.1038/nature08762.

22. Homentcovschi, S., and Higuchi-Sanabria, R. (2022). A neuron's ambrosia: non-autonomous unfolded protein response of the endoplasmic reticulum promotes lifespan. Neural Regen Res *17*, 309–310. https://doi.org/10.4103/1673-5374.317967.

23. Heifetz, A., Keenan, R.W., and Elbein, A.D. (1979). Mechanism of action of tunicamycin on the UDP-GlcNAc:dolichyl-phosphate Glc-NAc-1-phosphate transferase. Biochemistry *18*, 2186–2192. https://doi.org/10.1021/bi00578a008.

24. Morley, J.F., Brignull, H.R., Weyers, J.J., and Morimoto, R.I. (2002). The threshold for polyglutamine-expansion protein aggregation and cellular toxicity is dynamic and influenced by aging in Caenorhabditis elegans. Proceedings of the National Academy of Sciences *99*, 10417–10422. https://doi.org/10.1073/pnas.152161099.

25. Tan, M.-W., Mahajan-Miklos, S., and Ausubel, F.M. (1999). Killing of Caenorhabditis elegans by Pseudomonas aeruginosa used to model mammalian bacterial pathogenesis. Proceedings of the National Academy of Sciences *96*, 715–720. https://doi.org/10.1073/pnas.96.2.715.

26. Meisel, J.D., and Kim, D.H. (2014). Behavioral avoidance of pathogenic bacteria by *Caenorhabditis elegans*. Trends in Immunology *35*, 465–470. https://doi.org/10.1016/j.it.2014.08.008.

27. Zhang, Y., Lu, H., and Bargmann, C.I. (2005). Pathogenic bacteria induce aversive olfactory learning in Caenorhabditis elegans. Nature *438*, 179–184. https://doi.org/10.1038/nature04216.

28. O'Donnell, M.P., Fox, B.W., Chao, P.-H., Schroeder, F.C., and Sengupta, P. (2020). A neurotransmitter produced by gut bacteria modulates host sensory behaviour. Nature *583*, 415–420. https://doi.org/10.1038/s41586-020-2395-5.

29. Nair, T., Weathers, B.A., Stuhr, N.L., Nhan, J.D., and Curran, S.P. (2024). Serotonin deficiency from constitutive SKN-1 activation drives pathogen apathy. Preprint, https://doi.org/10.1101/2024.02.10.579755 https://doi.org/10.1101/2024.02.10.579755.

30. Egge, N., Arneaud, S.L.B., Wales, P., Mihelakis, M., McClendon, J., Fonseca, R.S., Savelle, C., Gonzalez, I., Ghorashi, A., Yadavalli, S., et al. (2019). Age-Onset Phosphorylation of a Minor Actin Variant Promotes Intestinal Barrier Dysfunction. Developmental Cell *51*, 587-601.e7. https://doi.org/10.1016/j.devcel.2019.11.001.

31. Garcia, G., Bar-Ziv, R., Averbukh, M., Dasgupta, N., Dutta, N., Zhang, H., Fan, W., Moaddeli, D., Tsui, C.K., Castro Torres, T., et al. (2023). Large-scale genetic screens identify BET-1 as a cytoskeleton regulator promoting actin function and life span. Aging Cell *22*, e13742. https://doi.org/10.1111/acel.13742.

32. Grant, B., and Hirsh, D. (1999). Receptor-mediated endocytosis in the Caenorhabditis elegans oocyte. Mol. Biol. Cell *10*, 4311–4326. https://doi.org/10.1091/mbc.10.12.4311.

33. Stevens, J., and Spang, A. (2013). N-glycosylation is required for secretion and mitosis in C. elegans. PLoS ONE *8*, e63687. https://doi.org/10.1371/journal.pone.0063687.

34. Na, H., Zhang, P., Chen, Y., Zhu, X., Liu, Y., Liu, Y., Xie, K., Xu, N., Yang, F., Yu, Y., et al. (2015). Identification of lipid droplet structure-like/resident proteins in Caenorhabditis elegans. Biochimica et Biophysica Acta (BBA) - Molecular Cell Research *1853*, 2481–2491. https://doi.org/10.1016/j.bbamcr.2015.05.020.

35. Zhang, P., Na, H., Liu, Z., Zhang, S., Xue, P., Chen, Y., Pu, J., Peng, G., Huang, X., Yang, F., et al. (2012). Proteomic study and marker protein identification of Caenorhabditis elegans lipid droplets. Mol. Cell Proteomics *11*, 317–328. https://doi.org/10.1074/mcp.M111.016345.

36. Du, J., Zhao, L., Kang, Q., He, Y., and Bi, Y. An optimized method for Oil Red O staining with the salicylic acid ethanol solution. Adipocyte *12*, 2179334. https://doi.org/10.1080/21623945.2023.2179334.

37. Frakes, A.E., and Dillin, A. (2017). The UPR(ER): Sensor and Coordinator of Organismal Homeostasis. Mol. Cell *66*, 761–771. https://doi.org/10.1016/j.molcel.2017.05.031.

38. Grootjans, J., Kaser, A., Kaufman, R.J., and Blumberg, R.S. (2016). The unfolded protein response in immunity and inflammation. Nat Rev Immunol *16*, 469–484. https://doi.org/10.1038/nri.2016.62.

39. Shen, X., Ellis, R.E., Sakaki, K., and Kaufman, R.J. (2005). Genetic interactions due to constitutive and inducible gene regulation mediated by the unfolded protein response in C. elegans. PLoS Genet. *1*, e37. https://doi.org/10.1371/journal.pgen.0010037.

40. Zhao, X., and Karpac, J. (2021). Glutamate metabolism directs energetic trade-offs to shape host-pathogen susceptibility in Drosophila. Cell Metabolism *33*, 2428-2444.e8. https://doi.org/10.1016/j.cmet.2021.10.003.

41. Randi, F., Sharma, A.K., Dvali, S., and Leifer, A.M. (2023). Neural signal propagation atlas of Caenorhabditis elegans. Nature *623*, 406–414. https://doi.org/10.1038/s41586-023-06683-4.

42. Mizunami, M., and Matsumoto, Y. (2017). Roles of Octopamine and Dopamine Neurons for Mediating Appetitive and Aversive Signals in Pavlovian Conditioning in Crickets. Front Physiol *8*, 1027. https://doi.org/10.3389/fphys.2017.01027.

43. Disorders, I. of M. (US) F. on N. and N.S. (2011). Overview of the Glutamatergic System. In Glutamate-Related Biomarkers in Drug Development for Disorders of the Nervous System: Workshop Summary (National Academies Press (US)).

44. Garcia, G., Homentcovschi, S., Kelet, N., and Higuchi-Sanabria, R. (2022). Imaging of Actin Cytoskeletal Integrity During Aging in C. elegans. In Cytoskeleton : Methods and Protocols, R. H. Gavin, ed. (Springer US), pp. 101–137. https://doi.org/10.1007/978-1-0716-1661-1_5.

45. Schindelin, J., Arganda-Carreras, I., Frise, E., Kaynig, V., Longair, M., Pietzsch, T., Preibisch, S., Rueden, C., Saalfeld, S., Schmid, B., et al. (2012). Fiji: an open-source platform for biological-image analysis. Nat Methods *9*, 676–682. https://doi.org/10.1038/nmeth.2019.

46. Egge, N., Arneaud, S.L.B., Wales, P., Mihelakis, M., McClendon, J., Fonseca, R.S., Savelle, C., Gonzalez, I., Ghorashi, A., Yadavalli, S., et al. (2019). Age-Onset Phosphorylation of a Minor Actin Variant Promotes Intestinal Barrier Dysfunction. Developmental Cell *51*, 587-601.e7. https://doi.org/10.1016/j.devcel.2019.11.001.

47. Grant, B., and Hirsh, D. (1999). Receptor-mediated Endocytosis in the Caenorhabditis elegans Oocyte. MBoC *10*, 4311–4326. https://doi.org/10.1091/mbc.10.12.4311.

48. Lord, S., Velle, K., Mullins, D., and Fritz-Laylin, L. (2020). SuperPlots: Communicating reproducibility and variability in cell biology. Journal of Cell Biology *219*, e202001064. https://doi.org/10.1083/jcb.202001064.

49. Stuhr, N., Nhan, J., Hammerquist, A., Van Camp, B., Reoyo, D., and Curran, S. (2022). Rapid Lipid Quantification in Caenorhabditis elegans by Oil Red O and Nile Red Staining. BIO-PROTOCOL *12*. https://doi.org/10.21769/BioProtoc.4340.

50. Lynn, D.A., Dalton, H.M., Sowa, J.N., Wang, M.C., Soukas, A.A., and Curran, S.P. (2015). Omega-3 and -6 fatty acids allocate somatic and germline lipids to ensure fitness during nutrient and oxidative stress in Caenorhabditis elegans. Proceedings of the National Academy of Sciences *112*, 15378–15383. https://doi.org/10.1073/pnas.1514012112.

51. Bray, N.L., Pimentel, H., Melsted, P., and Pachter, L. (2016). Near-optimal probabilistic RNA-seq quantification. Nat Biotechnol *34*, 525–527. https://doi.org/10.1038/nbt.3519.

52. Love, M.I., Huber, W., and Anders, S. (2014). Moderated estimation of fold change and dispersion for RNA-seq data with DESeq2. Genome Biol *15*, 550. https://doi.org/10.1186/s13059-014-0550-8.

53. Calfon, M., Zeng, H., Urano, F., Till, J.H., Hubbard, S.R., Harding, H.P., Clark, S.G., and Ron, D. (2002). IRE1 couples endoplasmic reticulum load to secretory capacity by processing the XBP-1 mRNA. Nature *415*, 92–96. https://doi.org/10.1038/415092a.

54. Chen, E.Y., Tan, C.M., Kou, Y., Duan, Q., Wang, Z., Meirelles, G.V., Clark, N.R., and Ma'ayan, A. (2013). Enrichr: interactive and collaborative HTML5 gene list enrichment analysis tool. BMC Bioinformatics *14*, 1–14. https://doi.org/10.1186/1471-2105-14-128.

55. Kuleshov, M.V., Jones, M.R., Rouillard, A.D., Fernandez, N.F., Duan, Q., Wang, Z., Koplev, S., Jenkins, S.L., Jagodnik, K.M., Lachmann, A., et al. (2016). Enrichr: a comprehensive gene set enrichment analysis web server 2016 update. Nucleic Acids Research *44*, W90–W97. https://doi.org/10.1093/nar/gkw377.

56. Stroustrup, N., Ulmschneider, B.E., Nash, Z.M., López-Moyado, I.F., Apfeld, J., and Fontana, W. (2013). The Caenorhabditis elegans Lifespan Machine. Nature Methods *10*, 665–670. https://doi.org/10.1038/nmeth.2475.

57. Torres, T.C., Moaddeli, D., Averbukh, M., Coakley, A.J., Dutta, N., Garcia, G., and Higuchi-Sanabria, R. (2022). Surveying Low-Cost Methods to Measure Lifespan and Healthspan in Caenorhabditis elegans. JoVE (Journal of Visualized Experiments), e64091. https://doi.org/10.3791/64091.

58. Cezairliyan, B., Vinayavekhin, N., Grenfell-Lee, D., Yuen, G.J., Saghatelian, A., and Ausubel, F.M. (2013). Identification of Pseudomonas aeruginosa Phenazines that Kill Caenorhabditis elegans. PLOS Pathogens *9*, e1003101. https://doi.org/10.1371/journal.ppat.1003101.

59. Mahajan-Miklos, S., Tan, M.-W., Rahme, L.G., and Ausubel, F.M. (1999). Molecular Mechanisms of Bacterial Virulence Elucidated Using a Pseudomonas aeruginosa–Caenorhabditis elegans Pathogenesis Model. Cell *96*, 47–56. https://doi.org/10.1016/S0092-8674(00)80958-7.

60. Stuhr, N.L., Ramos, C.M., Turner, C.D., Soukas, A.A., and Curran, S.P. (2024). C. elegans display antipathy behavior towards food after contemporaneous integration of nutritional

needs and dietary lipid availability. Preprint at bioRxiv, https://doi.org/10.1101/2024.02.23.581740 https://doi.org/10.1101/2024.02.23.581740.

61. Mohri-Shiomi, A., and Garsin, D.A. (2008). Insulin Signaling and the Heat Shock Response Modulate Protein Homeostasis in the Caenorhabditis elegans Intestine during Infection *. Journal of Biological Chemistry *283*, 194–201. https://doi.org/10.1074/jbc.M707956200.

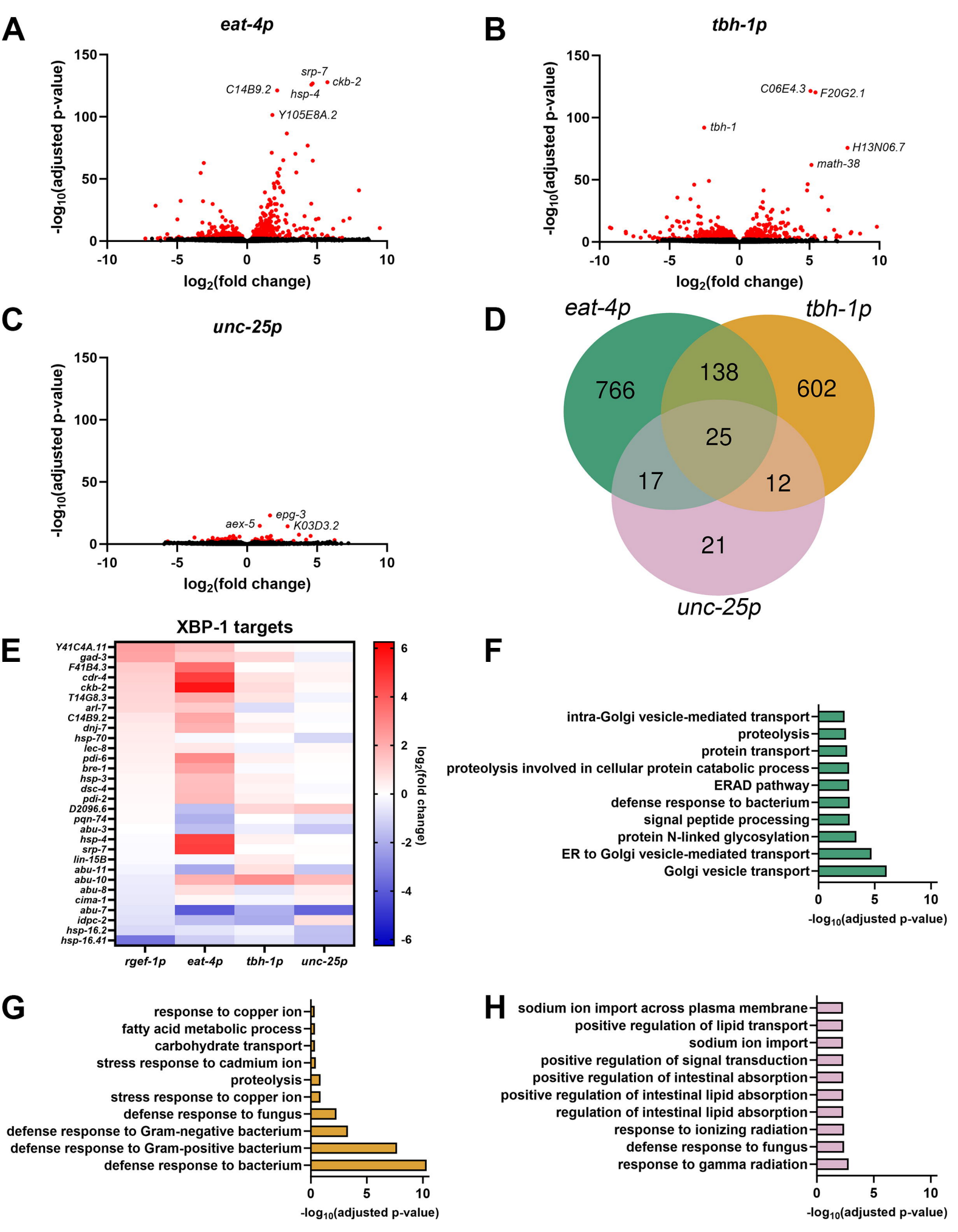
A
eat-4p
srp-7
ckb-2
C14B9.2
hsp-4
Y105E8A.2
-log10(adjusted p-value)
log2(fold change)
B
tbh-1p
C06E4.3
F20G2.1
tbh-1
H13N06.7
math-38
C
unc-25p
epg-3
aex-5
K03D3.2
D
eat-4p
tbh-1p
unc-25p
766
138
602
25
17
12
21
E
XBP-1 targets
Y41C4A.11
gad-3
F41B4.3
cdr-4
ckb-2
T14G8.3
arl-7
C14B9.2
dnj-7
hsp-70
lec-8
pdi-6
bre-1
hsp-3
dsc-4
pdi-2
D2096.6
pqn-74
abu-3
hsp-4
srp-7
lin-15B
abu-11
abu-10
abu-8
cima-1
abu-7
idpc-2
hsp-16.2
hsp-16.41
rgef-1p
eat-4p
tbh-1p
unc-25p
log2(fold change)
F
intra-Golgi vesicle-mediated transport
proteolysis
protein transport
proteolysis involved in cellular protein catabolic process
ERAD pathway
defense response to bacterium
signal peptide processing
protein N-linked glycosylation
ER to Golgi vesicle-mediated transport
Golgi vesicle transport
-log10(adjusted p-value)
G
response to copper ion
fatty acid metabolic process
carbohydrate transport
stress response to cadmium ion
proteolysis
stress response to copper ion
defense response to fungus
defense response to Gram-negative bacterium
defense response to Gram-positive bacterium
defense response to bacterium
-log10(adjusted p-value)
H
sodium ion import across plasma membrane
positive regulation of lipid transport
sodium ion import
positive regulation of signal transduction
positive regulation of intestinal absorption
positive regulation of intestinal lipid absorption
regulation of intestinal lipid absorption
response to ionizing radiation
defense response to fungus
response to gamma radiation
-log10(adjusted p-value)

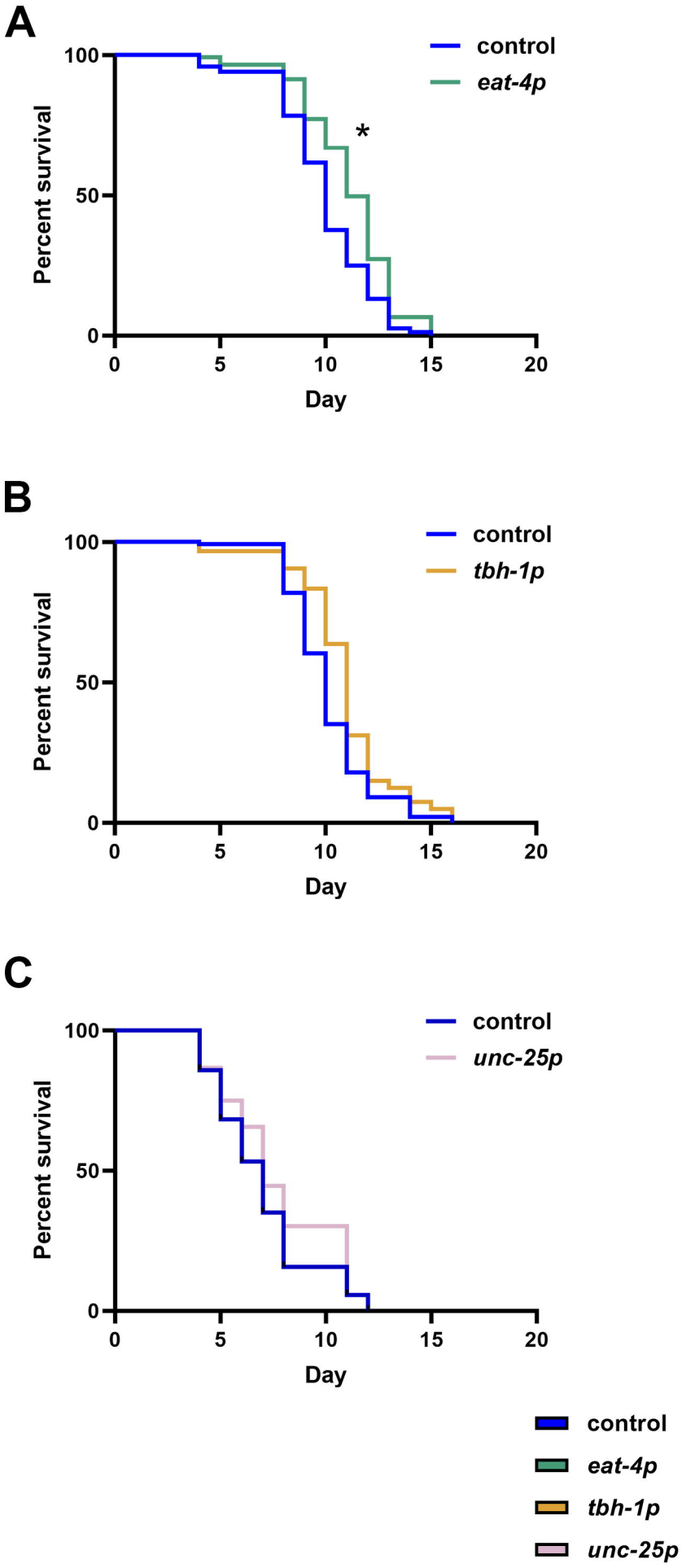
A
control
eat-4p
*
Percent survival
Day
B
control
tbh-1p
Percent survival
Day
C
control
unc-25p
Percent survival
Day
control
eat-4p
tbh-1p
unc-25p

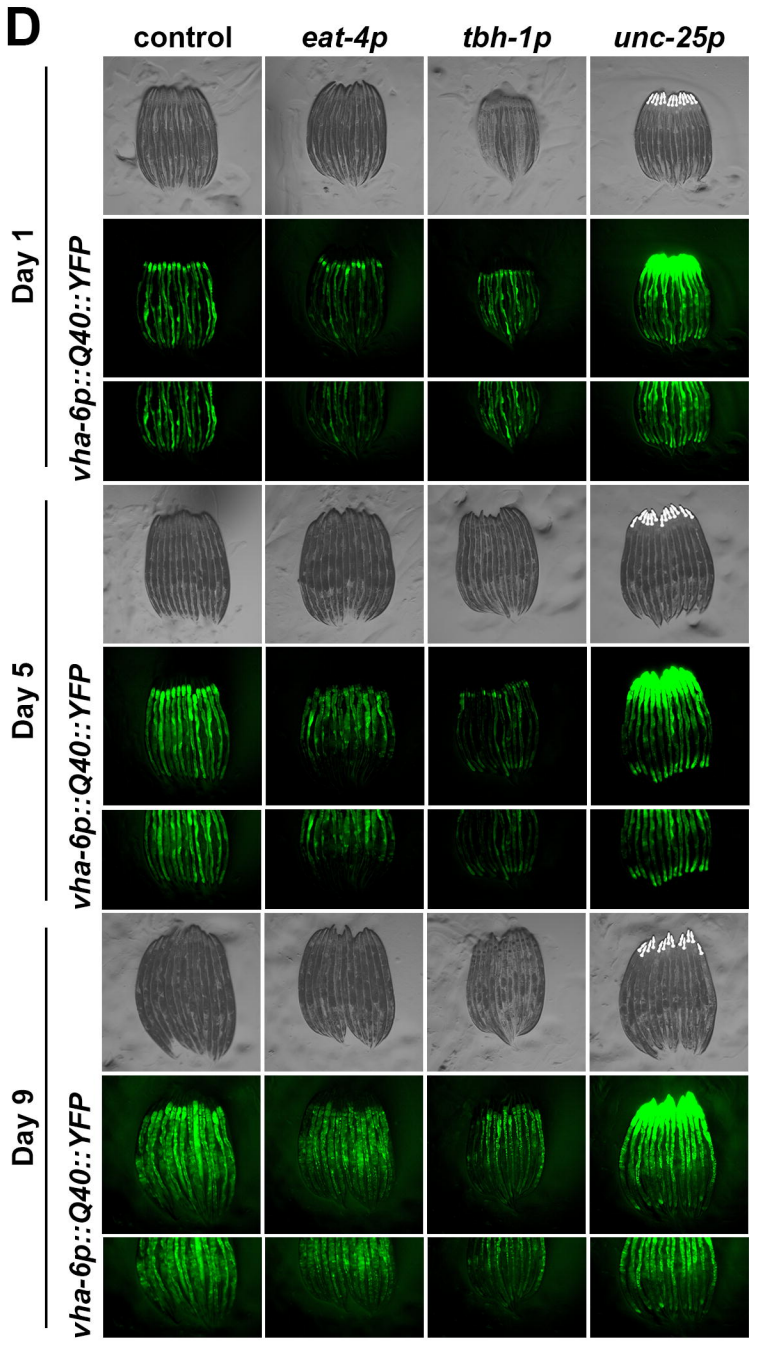
D
control
eat-4p
tbh-1p
unc-25p
Day 1
Day 5
Day 9
vha-6p::Q40::YFP

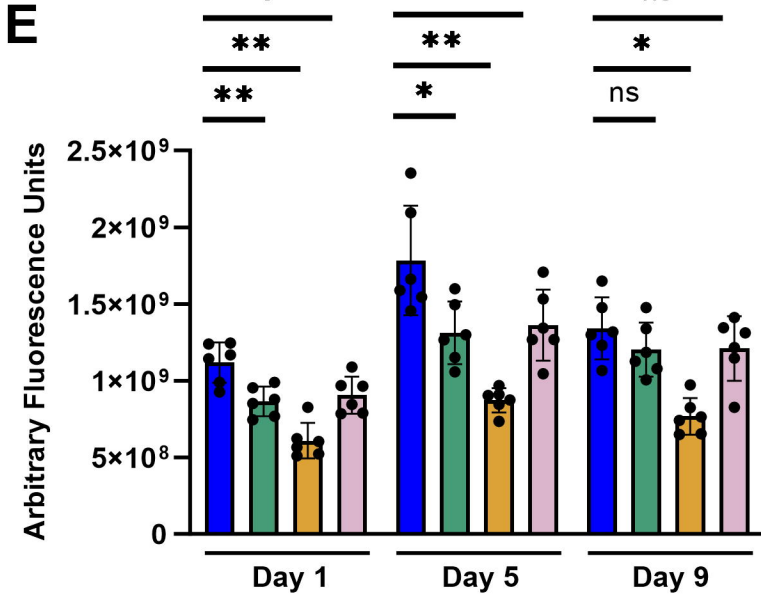
E
*
**
**
*
**
*
ns
*
ns
Arbitrary Fluorescence Units
2.5×10⁹
2×10⁹
1.5×10⁹
1×10⁹
5×10⁸
0
Day 1
Day 5
Day 9

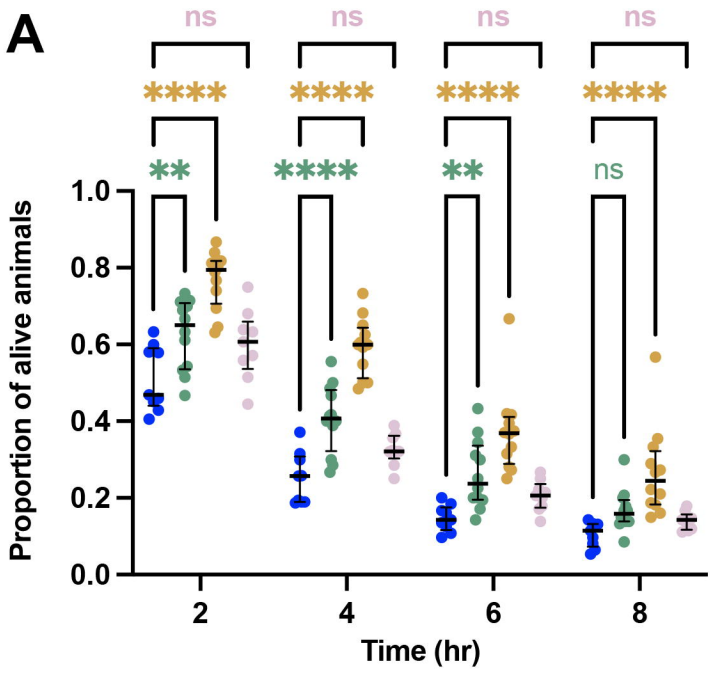
A
ns
ns
ns
ns
****
****
****
****
**
****
**
ns
Proportion of alive animals
1.0
0.8
0.6
0.4
0.2
0.0
2
4
6
8
Time (hr)

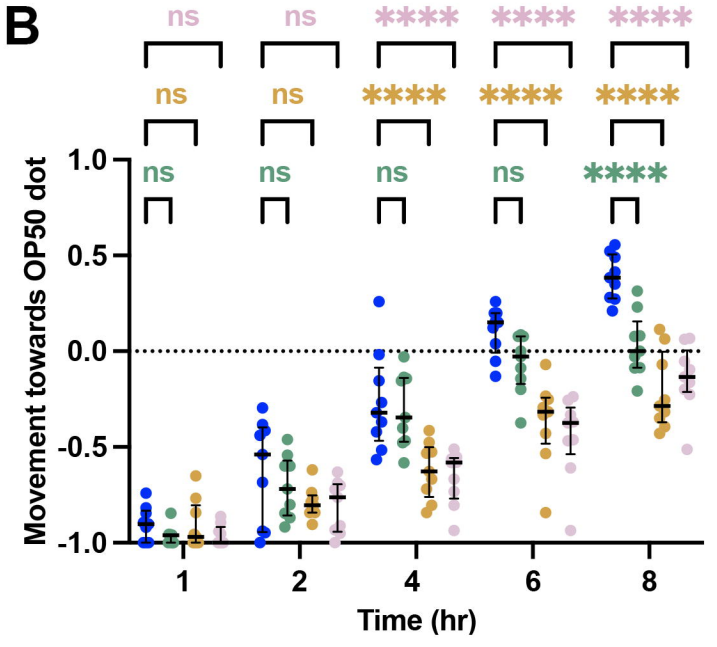
B
ns
ns
****
****
****
ns
ns
****
****
****
ns
ns
ns
ns
****
Movement towards OP50 dot
1.0
0.5
0.0
-0.5
-1.0
1
2
4
6
8
Time (hr)

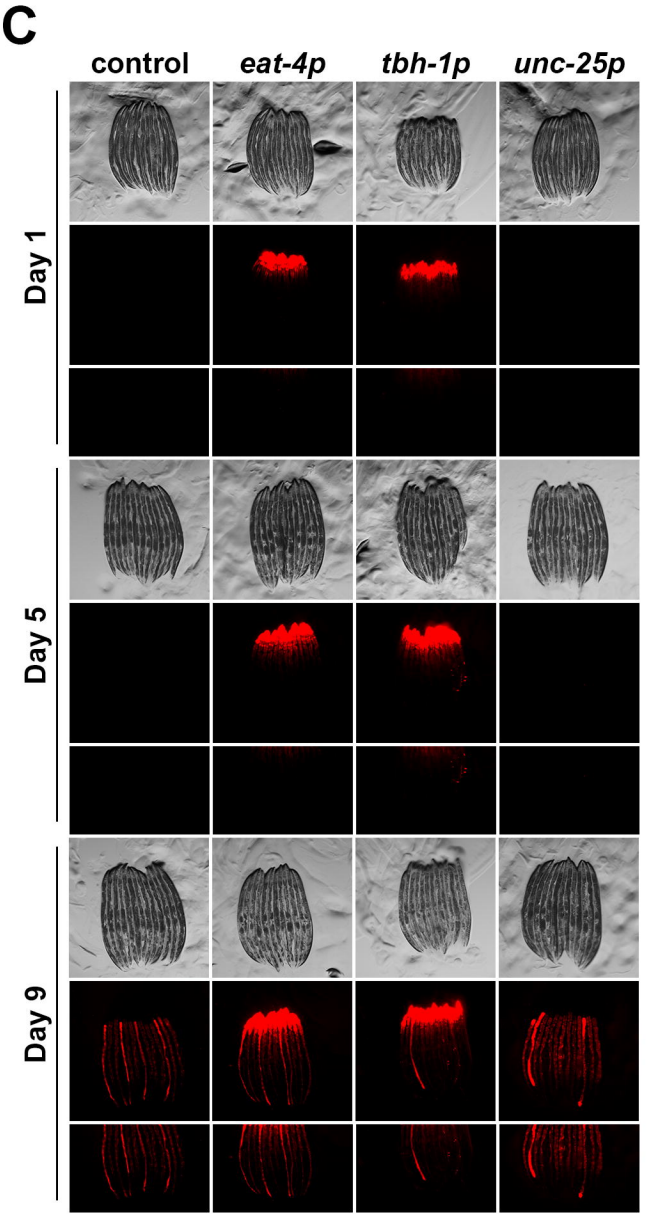
C
control
eat-4p
tbh-1p
unc-25p
Day 1
Day 5
Day 9

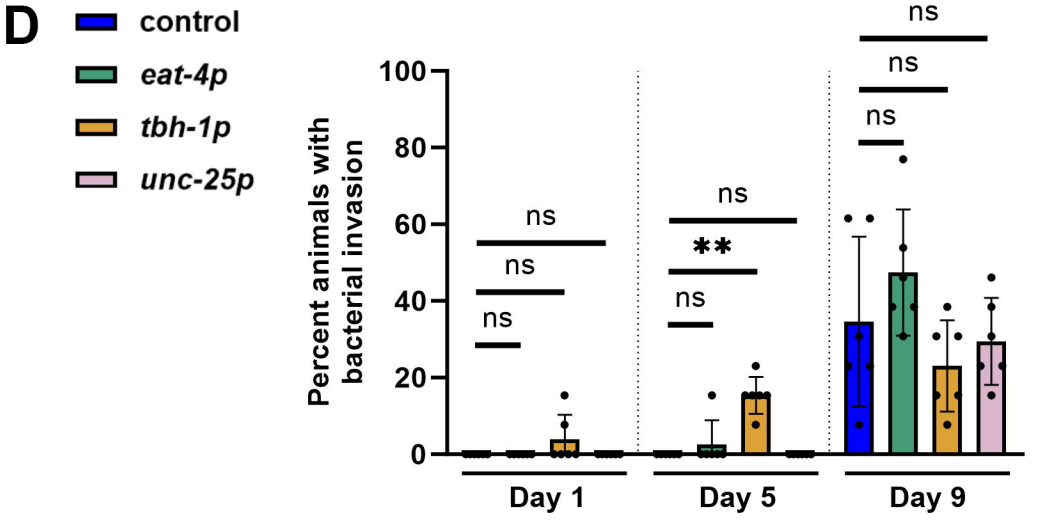
D
control
eat-4p
tbh-1p
unc-25p
Percent animals with bacterial invasion
100
80
60
40
20
0
ns
ns
ns
ns
**
ns
ns
ns
ns
Day 1
Day 5
Day 9

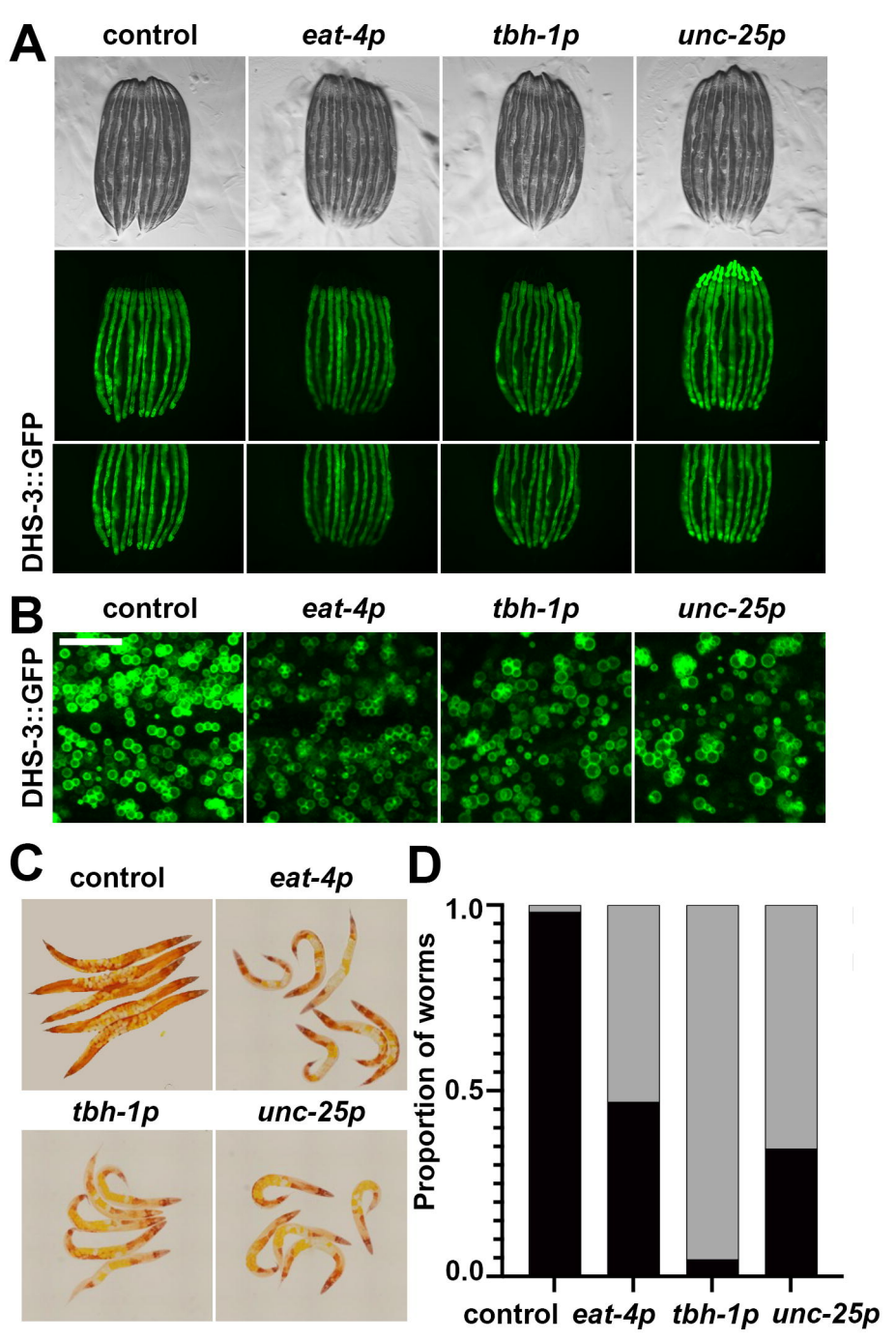
A
control
eat-4p
tbh-1p
unc-25p
DHS-3::GFP
B
control
eat-4p
tbh-1p
unc-25p
DHS-3::GFP
C
control
eat-4p
tbh-1p
unc-25p
D
Proportion of worms
1.0
0.5
0.0
control
eat-4p
tbh-1p
unc-25p

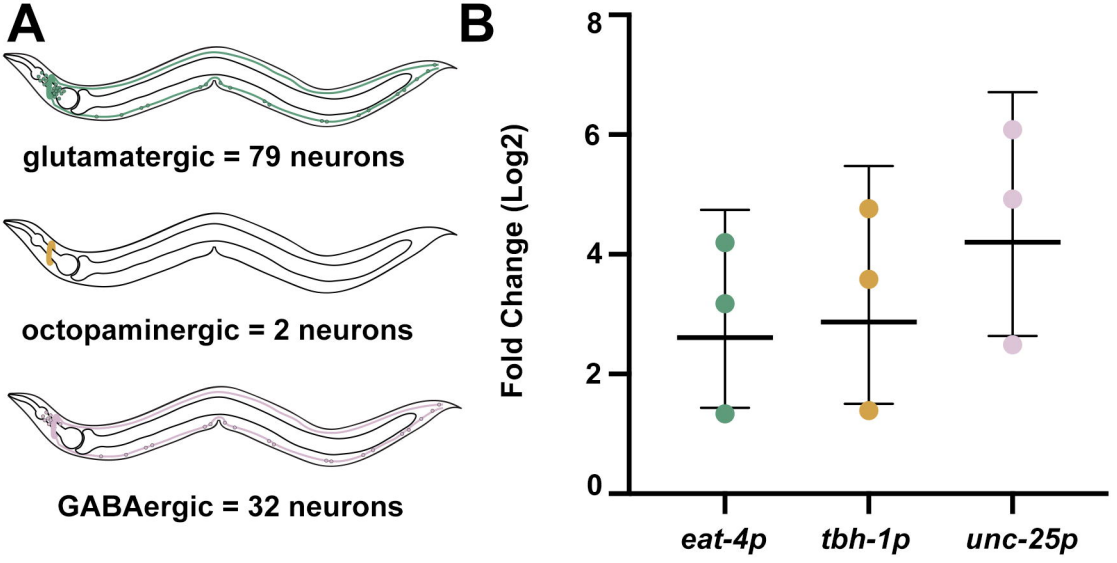
A
glutamatergic = 79 neurons
octopaminergic = 2 neurons
GABAergic = 32 neurons
B
Fold Change (Log2)
8
6
4
2
0
eat-4p
tbh-1p
unc-25p

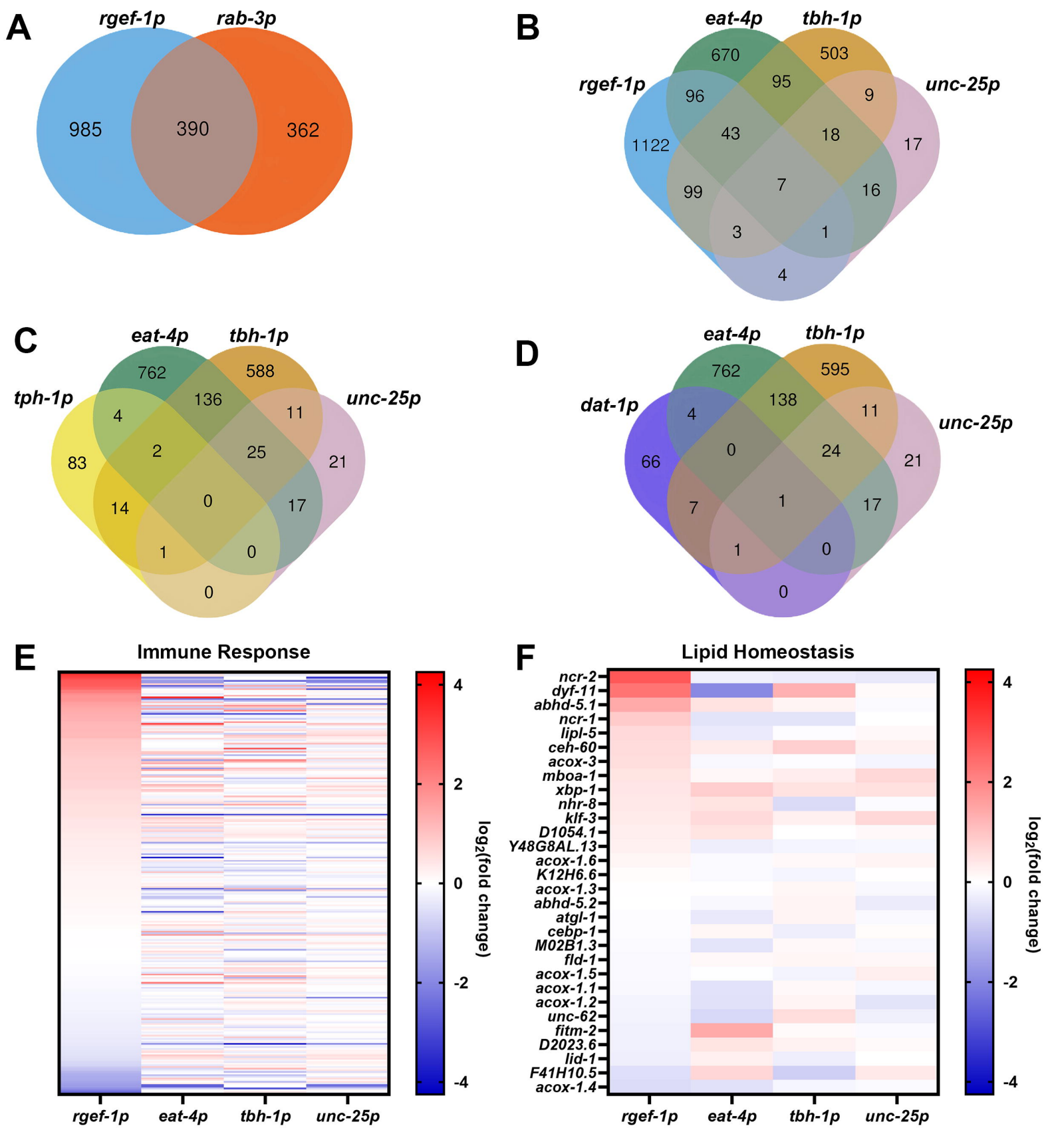
A
rgef-1p
rab-3p
985
390
362
B
eat-4p
tbh-1p
rgef-1p
unc-25p
670
503
96
95
9
1122
43
18
17
99
7
16
3
1
4
C
eat-4p
tbh-1p
tph-1p
unc-25p
762
588
4
136
11
83
2
25
21
14
0
17
1
0
0
D
eat-4p
tbh-1p
dat-1p
unc-25p
762
595
4
138
11
66
0
24
21
7
1
17
1
0
0
E
Immune Response
rgef-1p
eat-4p
tbh-1p
unc-25p
4
2
0
-2
-4
log2(fold change)
F
Lipid Homeostasis
ncr-2
dyf-11
abhd-5.1
ncr-1
lipl-5
ceh-60
acox-3
mboa-1
xbp-1
nhr-8
klf-3
D1054.1
Y48G8AL.13
acox-1.6
K12H6.6
acox-1.3
abhd-5.2
atgl-1
cebp-1
M02B1.3
fld-1
acox-1.5
acox-1.1
acox-1.2
unc-62
fitm-2
D2023.6
lid-1
F41H10.5
acox-1.4
rgef-1p
eat-4p
tbh-1p
unc-25p
4
2
0
-2
-4
log2(fold change)

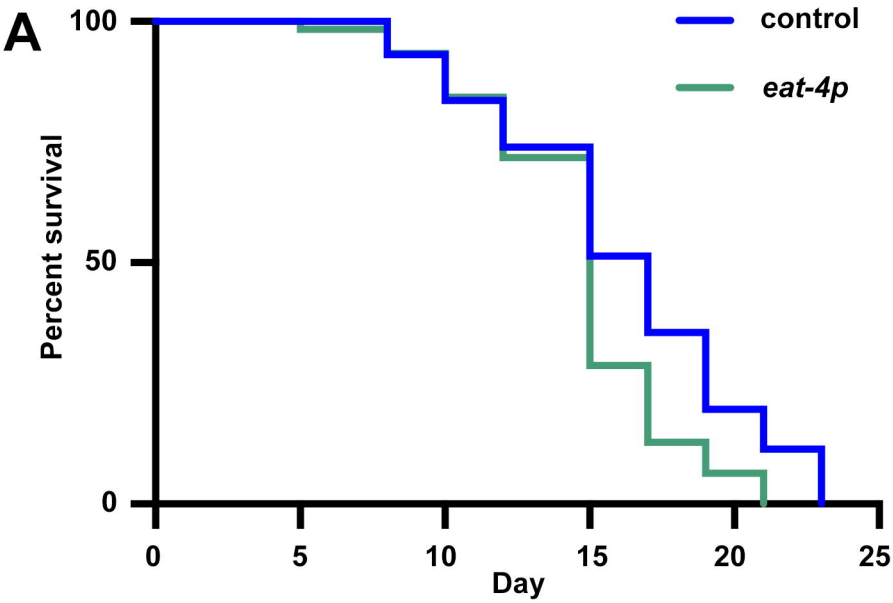
A
100
50
0
Percent survival
0
5
10
15
20
25
Day
control
eat-4p

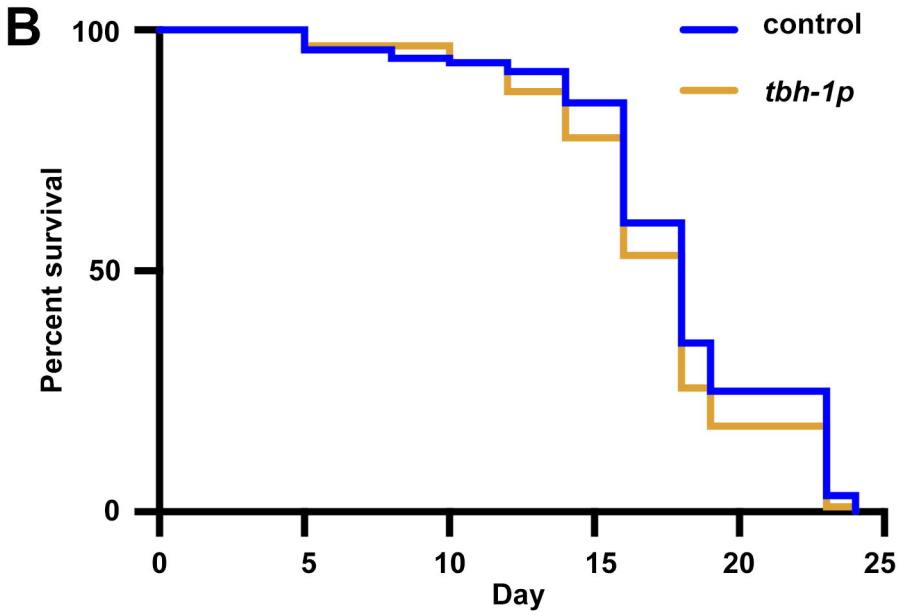
B
100
50
0
Percent survival
0
5
10
15
20
25
Day
control
tbh-1p

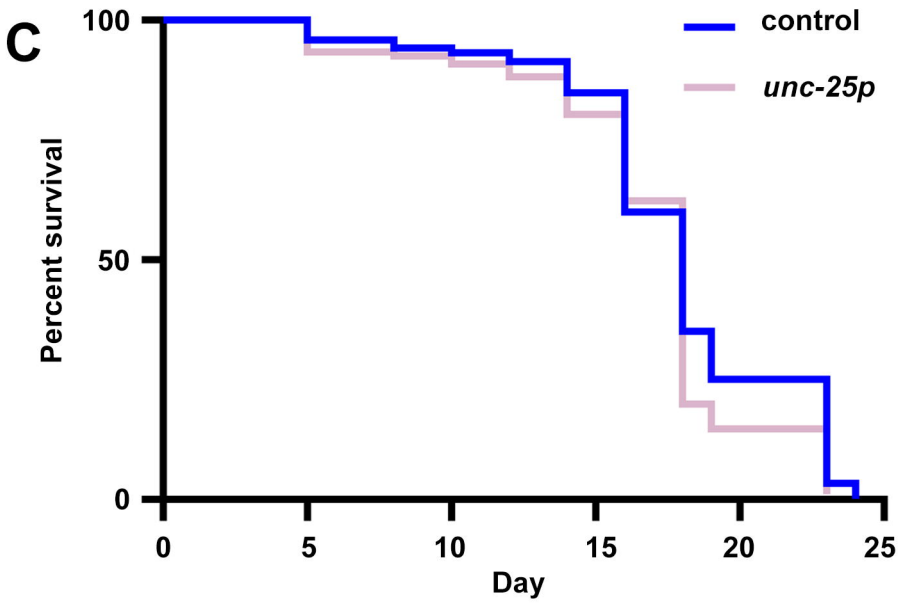
C
100
50
0
Percent survival
0
5
10
15
20
25
Day
control
unc-25p

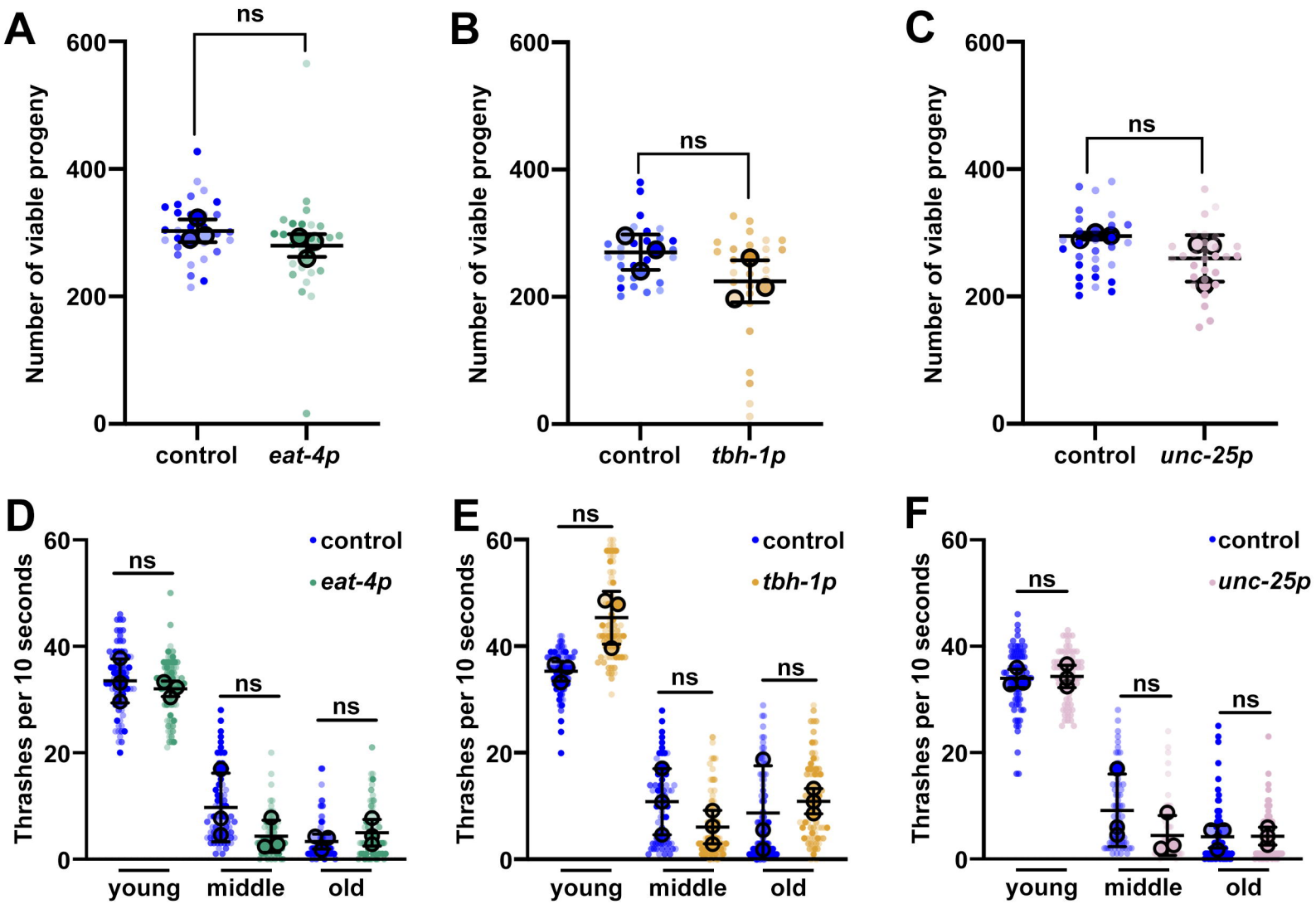
A
B
C
D
E
F
ns
Number of viable progeny
600
400
200
0
control
eat-4p
tbh-1p
unc-25p
Thrashes per 10 seconds
60
40
20
young
middle
old

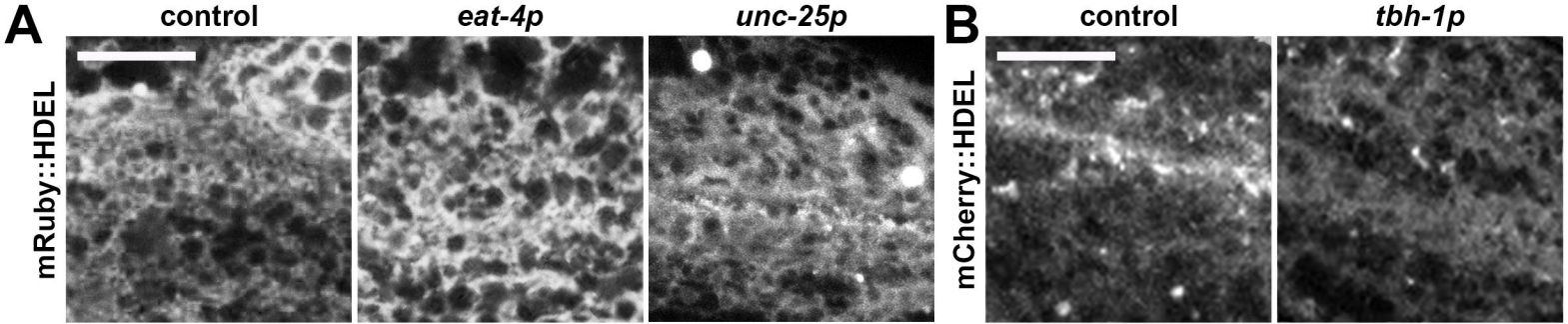
A
control
eat-4p
unc-25p
mRuby::HDEL
B
control
tbh-1p
mCherry::HDEL

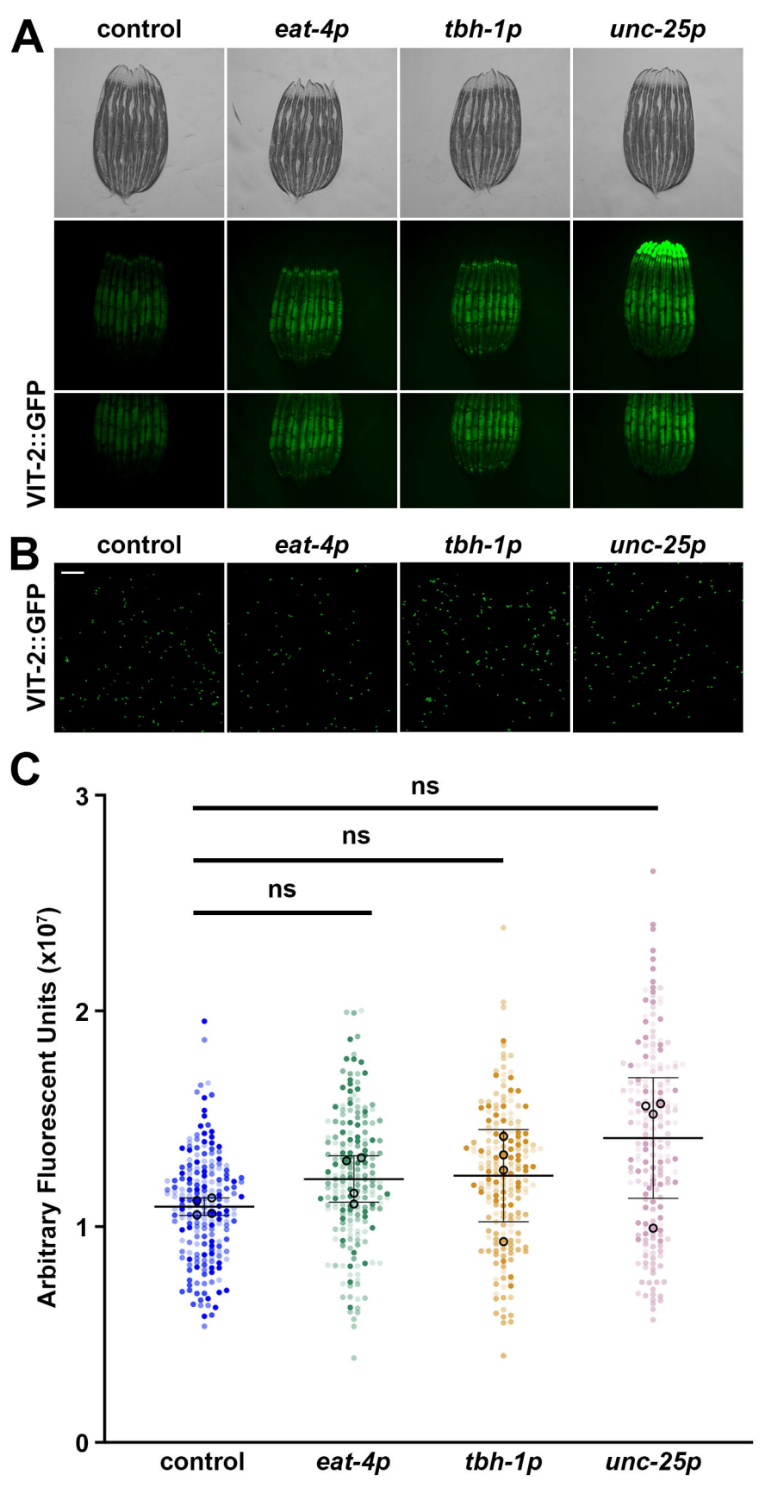
A
control
eat-4p
tbh-1p
unc-25p
VIT-2::GFP
B
control
eat-4p
tbh-1p
unc-25p
VIT-2::GFP
C
ns
ns
ns
Arbitrary Fluorescent Units (x10^7)
3
2
1
0
control
eat-4p
tbh-1p
unc-25p